

Review

Remote Sensing of Snow Cover Using Spaceborne SAR: A Review

Ya-Lun S. Tsai ^{1,*} , **Andreas Dietz** ¹, **Natascha Oppelt** ²  and **Claudia Kuenzer** ¹¹ German Remote Sensing Data Center (DFD), German Aerospace Center (DLR), Muenchener Strasse 20, D-82234 Wessling, Germany; Andreas.Dietz@dlr.de (A.D.); Claudia.Kuenzer@dlr.de (C.K.)² Department of Geography, Earth Observation and Modelling, Kiel University, Ludewig-Meyn-Str. 14, 24118 Kiel, Germany; oppelt@geographie.uni-kiel.de

* Correspondence: tsai.l.yalun@gmail.com

Received: 23 April 2019; Accepted: 14 June 2019; Published: 19 June 2019



Abstract: The importance of snow cover extent (SCE) has been proven to strongly link with various natural phenomenon and human activities; consequently, monitoring snow cover is one the most critical topics in studying and understanding the cryosphere. As snow cover can vary significantly within short time spans and often extends over vast areas, spaceborne remote sensing constitutes an efficient observation technique to track it continuously. However, as optical imagery is limited by cloud cover and polar darkness, synthetic aperture radar (SAR) attracted more attention for its ability to sense day-and-night under any cloud and weather condition. In addition to widely applied backscattering-based method, thanks to the advancements of spaceborne SAR sensors and image processing techniques, many new approaches based on interferometric SAR (InSAR) and polarimetric SAR (PolSAR) have been developed since the launch of ERS-1 in 1991 to monitor snow cover under both dry and wet snow conditions. Critical auxiliary data including DEM, land cover information, and local meteorological data have also been explored to aid the snow cover analysis. This review presents an overview of existing studies and discusses the advantages, constraints, and trajectories of the current developments.

Keywords: synthetic aperture radar; backscattering; InSAR; PolSAR; snow classification; wet snow; cryosphere; data fusion; machine learning

1. Introduction

Snow covered areas influence the global radiation balance, groundwater, runoff, glaciers, flora and fauna, and human activities such as tourism, civil engineering, and infrastructure. Within all cryospheric components, snow covers the widest area: During the wintertime, more than 40% of the northern hemisphere is covered by snow [1–3]. As a result of its multiple influences on the environment, snow cover is addressed in the Fifth Assessment Report (AR5) of the Intergovernmental Panel on Climate Change (IPCC) and is identified as a critical climate variable within the Global Climate Observing System (GCOS) [4]. Several snow cover projects relying on remote sensing have been conducted in recent years, including the European Space Agency (ESA)'s Satellite Snow Product Intercomparison and Evaluation Exercise (SnowPEx) [5], the German Aerospace Center (DLR)'s Global SnowPack [6], the National Aeronautics and Space Administration (NASA)'s Snow Experiment (SnowEx) [7], and the ongoing ESA's Let It Snow project [8] as well as new Climate Change Initiative Extension (CCI+) Essential Climate Variables (ECV) mission [9]. Figure 1 gives an overview of some of the aspects related to snow cover, and also illustrates some of the more variable snow cover characteristics such as liquid water content, grain size, density, and snow water equivalent (SWE).

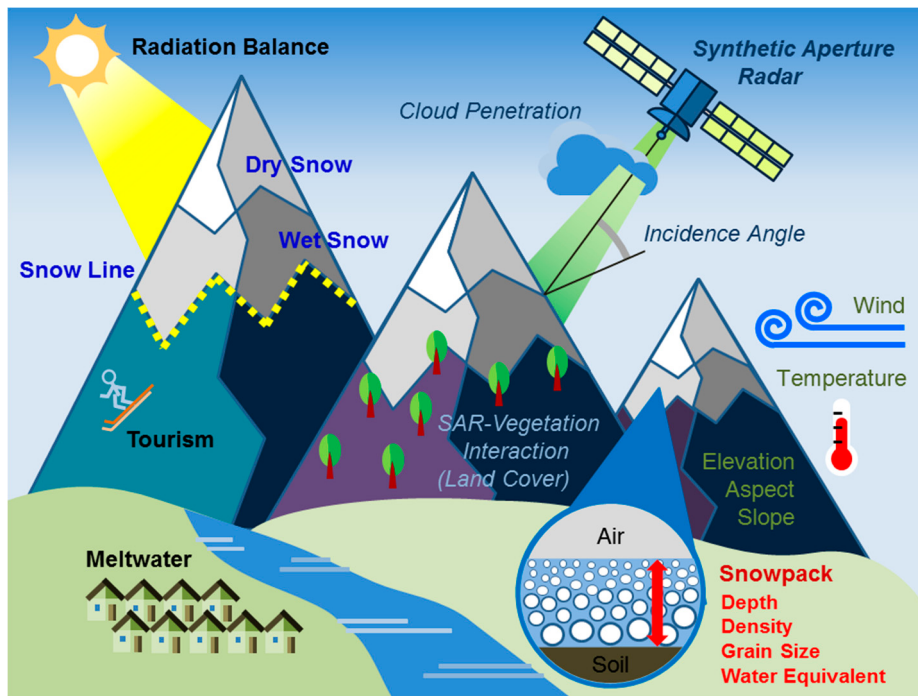


Figure 1. Illustration of different snow types and snow line (deep blue font), the importance of snow (black font), synthetic aperture radar (SAR)-related characteristics (font in italics), factors influence snow (green font) and snowpack parameters (red font).

Snow cover reflects incoming solar radiation, as fresh snow normally has an albedo between 0.8 and 0.9 while most land surfaces have an albedo ranging between 0.1 and 0.3 [10]; therefore, snow influences the regional and global energy balance [11–13]. A decrease in snow cover extent (SCE) and duration leads to a reduced albedo of the land surface, which increases the warming process and further accelerates the snowmelt process [14–18]. Additionally, snow cover affects the conditions and spatial distribution of other cryosphere components [19]: Snow is a prerequisite for temperate glaciers, controlling their equilibrium. The high albedo of snow preserves the retention of sea and lake ice and also influences the growth rate of ice thickness due to thermodynamic processes (freezing and melting) and snow types (dry or wet) [20–22]. Snow also interacts with permafrost due to its thermal insulation characteristic, which reduces the scale of variation of active layer thickness (ALT) caused by air temperature changing [23–25]. Consequently, snow cover is regarded as one of the most critical factors affecting the thermal regime of permafrost [26,27].

In addition, snow cover directly affects ecology and the socioeconomic system. Studies suggested that water originating from snowmelt dominates the runoff regimes of downstream regions not only in terms of water amount but also in distribution, quality, and seasonality [28–32]. Therefore it also controls the available water resources for the inhabiting population. More than 50% of precipitation in mountainous regions is falling as snow in Norway, the French Alps, and also the northern and western United States [13,33–37]. Moreover, snow cover and snowmelt in particular can also lead to natural disasters such as floods or avalanches (or in the absence of snow: Droughts). In order to identify possible flood events, detecting the onset of snowmelt in time is necessary [38–42]. Furthermore, snow cover is also an important aspect for winter tourism [43,44].

Due to global warming, a significant decrease in spring SCE has been shown in both observations and models [45–51], and recorded in the Synthesis Report of IPCC AR5 [52]. Climate change influences the global snow cover spatial extent as well as the duration. Beniston et al. [23] concluded that temperature increase as well as large-scale atmospheric patterns is the most influencing factors changing global snow cover. Snow cover onset and melt dates are shifting, generally leading to shorter snow cover seasons with later onset and earlier melt [53] although these general patterns can vary

on a regional scale [54,55]. On a global scale, winter precipitation has been shifting from snow to rainfall, which is particularly evident in regions with a more maritime climate [47]. In mountain regions, the effects of climate change on snow cover are even more significant, leading to an apparent decrease of SCE and duration [23,56,57]. Studies predicted that in the highest altitudes of the European Alps, SWE may be reduced to less than 20% of the present level by 2100 and that they may become totally snow-free in summertime [58,59]. As a result of all these aspects, continuously monitoring of snow cover is crucial.

Considering the wide areal coverage, temporal variability, inaccessibility and remote location of many snow covered regions, remote sensing is an ideal data acquisition technique for monitoring snow cover and its trends and developments on both spatial and temporal scales. Although the utilization of optical/multispectral remote sensing data for monitoring SCE has a long history compared to synthetic aperture radar (SAR) data [60,61], as data from optical sensors can be affected by cloud cover as well as (polar) darkness, spaceborne SAR data offers a valuable alternative for monitoring snow cover as it is independent from clouds and illumination conditions. Due to the availability of new SAR satellites during the recent decades together with the developments of the SAR-based SCE detection algorithms, more studies have tried to detect SCE based on SAR imagery instead of optical sensors. However, there has been no comprehensive discussion of current SAR-based SCE detection approaches' theories, technical limitations, critical auxiliary data, and the so far developing trajectory as well as future possibilities. Thus, in the following sections we therefore summarize the currently available techniques to detect snow cover utilizing SAR data and thoroughly compare their advantages and drawbacks.

2. Characteristics of Snow and SAR

2.1. SAR Sensor Characteristics

Radar remote sensing is an active sensing approach, which transmits electromagnetic (EM) radiation with wavelengths between 0.3 to 0.01 m and senses their echoes from the Earth surface [62,63]. The spatial resolution of the acquired imagery is approximately equal to one-half the length of the actual antenna and is independent from platform altitude [64]. Comparing to other contemporary active spaceborne sensors such as scatterometers, SAR is therefore able to monitor with higher spatial resolution and thus preserves more ground surface details.

Due to its active and relatively long wavelength characteristics, SAR does not rely on solar illumination and can therefore operate both day and night. SAR can also penetrate clouds, enabling measurements of the surface under all weather and illumination conditions. These abilities are particularly valuable when it comes to snow cover monitoring, as snow-covered alpine regions are often covered by clouds and high latitudes regions are affected by polar darkness during winter [65]. Furthermore, longer wavelengths of SAR can penetrate into the snowpack [66], potentially providing information about snowpack conditions such as snow grain size and SWE (liquid/frozen water content), and can even penetrate the frozen layer on the top surface of snow [67].

Owing to the unique sensing characteristics of SAR, the snow information recorded in SAR imagery is fundamentally different when compared to optical/multispectral imagery. The former records surface characteristics related to the roughness and dielectric properties; the latter records the reflection/absorption of the incoming solar irradiation at the top layer of the surface [68]. As snow, ice, and clouds are characterized by comparatively similar reflection properties in the visible and—depending on the cloud phase—the near to medium infrared part of the spectrum, confusions can occur when attempting to classify snow cover and discriminate it from ice or clouds [69,70]. SAR sensors can overcome this ambiguity as they measure surface properties in a different realm in terms of a backscatter coefficient, which is a function of the wavelength of the SAR signal, and the roughness and dielectric properties of the surface rather than the reflection properties.

An additional advantage of SAR sensors is derived from the phase information they record. Different polarizations (horizontal, vertical) allow for the detection of additional physical characteristics of the surface, such as shape, material, or angle of an observed target. Furthermore, based on the phase information recorded by SAR, coherence and interferometry can be generated [71–73], which can indicate the deformation and stability of ground features. Such information can be analyzed to detect and quantify, e.g., glacier velocity or other moving targets [74–76].

However, SAR also has some practical drawbacks for cryospheric application. The first is the comparatively low temporal resolution (i.e., revisit days, often longer than five days) when compared to operational optical/multispectral missions due to the trade-offs of orbit design including spatial resolution, tilt angle, swath width [77–79]. Based on the cryosphere report given by the Global Climate Observing System (GCOS) [80], the minimum requirement in terms of temporal resolution for spaceborne snowmelt area products for subsequent research of hydrology and climate is one to five days. Current optical/multispectral missions are designed with shorter, even daily revisiting time (e.g., Advanced Very High Resolution Radiometer (AVHRR), Moderate Resolution Imaging Spectroradiometer (MODIS), Sentinel-3A/B). Even though the temporal resolution is yet insufficient to provide daily imagery, the spatial resolution of recent SAR missions such as Sentinel-1 (5×20 m) is more than satisfactory, given that the minimum requirements expressed by GCOS are between 100 and 500 m.

Contrary to optical sensors, the geometry of SAR observations is more complex due to their synthesized multi-beam echoes transmitted and received at both, side-looking slant-range direction and azimuth direction [81]. The significance and type of the resulting distortions varies by landscape and sensing angle and thus leads to foreshortening, layover and shadow effects [82]. In addition, as the received signal for each pixel of the SAR imagery is the sum of the random constructive and destructive phase interferences reflected from countless ground features, the resultant speckles can degrade the image quality considerably [82,83]. Consequently, the interpretation and analysis of SAR images are more challenging than conventional optical observations.

The overview of different characteristics of SAR and optical sensors as well as advantages and drawbacks for snow cover monitoring are summarized in Table 1 and illustrated in Figure 1.

Table 1. Comparison of SAR and optical/multispectral sensors regarding their ability to detect snow cover.

Sensor	SAR	Optical/Multispectral
Sensing mode	Active	Passive
Wavelengths	0.01~0.3 m	0.3~1 μ m
Spatial resolution	PALSAR-2: 3~10 m COSMO-SkyMed: 3~15 m Sentinel-1: 5 \times 20 m (Stripmap mode)	Landsat-8: 15~30 m Sentinel-2: 10~20 m MODIS: 250~500 m (not included thermal band)
Temporal resolution	PALSAR-2: 14 days COSMO-SkyMed: ~5 days Sentinel-1: 6 days	Landsat-8: 16 days Sentinel-2: 5 days MODIS: 1 day
Recorded snow characteristics	Surface roughness, dielectric property	Surface reflection
Advantages	Day-and-night sensing under any weather condition; Possibility of interferometric and polarimetric information	Visually natural to interpret; High temporal resolution; Maturity of classification algorithms
Drawbacks	Low temporal resolution; Challenging to interpret due to its imaging geometry; Significant geometric distortions and speckles	Hindered by cloud, darkness; Confusion between snow, ice, and cloud

2.2. Interactions of Snow and SAR

Due to the penetration characteristics of the SAR signal, wet and dry snow behaves differently in SAR imagery. Practically, there are two different definitions of dry and wet snow. The first one is based on volume water content (VWC), i.e., a snowpack with VWC above 1% is considered wet snow, while snow below 1% VWC is referred to as dry snow [84]. The second definition, which is used more often, is connected to the temperature of the snowpack: At temperatures below 0 °C the snowpack is presumed to remain dry while above 0 °C the snow is considered wet [35,85,86]. The temperature definition was validated by statistical analysis of wet snow temperatures and proven advantageous when compared to the VWC approach, as measurements of temperature are easier to obtain than of VWC [85].

SAR observations of wet snow differ greatly from those of dry snow. As mentioned in Section 2.1, SAR signals can penetrate into the snowpack with the penetration depth depending on the wavelength of the signal. C-band SAR, for example, has a potential penetration depth of around 20 m when observing dry snow [87]. Since the grain size of snow is between 0.1 and 0.3 mm [88], the SAR signal with its much longer wavelengths passes through the snow crystals nearly unhindered, preventing any kind of backscattering reflection from the snow crystals [89,90]. As the snowpack begins to melt, the dielectric properties of the snowpack change considerably, decreasing the penetration depth to around 3 cm while backscattering reflection from the liquid water becomes the dominant process [87,91–96]. At a frequency higher than 1 MHz, the dielectric constants of air, ice, and water are 1.0, 3.17 ± 0.07 and 80, respectively [97]. As the proportions of air, ice, and water within a snowpack change when melting begins, the cumulative dielectric constant also changes, leading from initially low values between 1.2 and 2.0 to much higher values [30,98,99].

Additionally, the liquid water content of a snowpack also affects the scattering mechanism, i.e., how the multi-layered snowpack reflects the incoming SAR signal. Under dry snowpack conditions, the dominant scattering process is the sum of volume scattering of the snowpack and the surface scattering at the snow/ground interface. When the snowpack becomes wet, the surface scattering at the air/snow interface dominates the scattering mechanism [92,100–103].

However, as the snowpack is a complex multi-layer structure, snow grain size, density, depth, stratigraphy, amount of impurities and surface roughness may affect its backscattering [104,105]. Surface and volume scattering is proportional to the polarization amplitude and transmissivity of the snowpack, respectively. The dielectric constant and local incidence angle (LIA) also affect the transmissivity [106]. Table 2 presents an overview of each factor's influence on the scattering of dry and wet snow as well as the backscattering characteristics. However, it must be noted that many factors affect scattering mechanisms, such as radar wavelength, polarization, incidence angle, surface roughness, and dielectric properties [107–111]. Longer wavelengths will produce more volume scattering due to a deeper penetration [112].

Table 2. Effects of wet and dry snow on the SAR signal based on the snow physiology. “+” refers to positive correlation, “−” to negative correlation. The number in brackets refers to the reference number.

Snow Type	Dry Snow	Wet Snow
Backscattering source	Volume scattering from snowpack, Surface scattering at snow/ground interface	Surface scattering at air/snow interface
Dominant factors influencing scattering mechanism [113]	Surface below snow (SAR frequency $<\sim 10$ GHz), Grain size (SAR frequency $> \sim 10$ GHz)	Liquid water content (most important), Surface roughness
Backscattering coefficient	High	Low
The relationship between snowpack parameters and the amplitude of backscattering		
Snow wetness	−[114]	+[92,99,115]
Snow grain size	+[106,116]	insignificant [117]
Snow depth/thickness	+coarse-grained snowpack [96] −fine-grained snowpack [96]	−[117]

3. SAR-Based Studies and Methods to Detect Snow

The launch of SeaSat in 1978 initiated the era of utilizing spaceborne SAR sensors for global snow cover monitoring. While some snow-related studies were published with SeaSat's L-band SAR [119,120], studying snow cover with SAR data has become more mature since the launch of the first continuously revisiting ERS-1 (C-band) in 1991 as ERS-1 providing the opportunity to use repeat-pass multi-temporal observations, which minimizes the influence of topographic effects on the backscattering by ensuring similar sensing geometry [121] and thus produces more reliable snow cover estimations.

Consequently, the following literature review includes the results and findings from 96 snow cover studies mapping SCE with spaceborne SAR sensors after the launch of ERS-1, selected from commonly used academic search engines including Google Scholar, Web of Science, and Scopus. Studies focusing on SWE and snow depth (SD) have been excluded from the review. Airborne-based studies are also excluded from this compilation as their temporal and spatial scopes are often limited by the mission design and thus, their insights are often not universally transferrable. The number of available publications since 1992 clearly has shown an upward trend. This implies that the present status of SAR-based snow cover monitoring is still in a developing stage [106,122].

3.1. SAR Sensors Used for Detecting Snow

Figure 2 presents an overview of commonly used spaceborne SAR sensors including their operation time span and band information. C-band SAR sensors stands out due to the longest available time series of continuous observations since 1992, which mainly thanks to the ESA's and Canadian Space Agency (CSA)'s missions, featuring ESA's pioneering ERS-1/2, Envisat, CSA's Radarsat-1/2, and the ESA milestone missions of Sentinel-1. The pioneering Active Microwave Instrumentation (AMI) C-band instrument equipped on oceanographic research-aimed ERS-1 satellite starts the era of C-band SAR for the following decades, although it was only aimed at aiding the scatterometer for deriving ocean wind and wave information [123]. Together with the subsequent ESA's C-band missions, there have been a seamless time series of C-band imagery for more than 20 years. This time series became the most commonly used dataset for analyzing snow cover from SAR as the characteristics of C-band SAR is suitable for snow detection and the interchangeability of each C-band SAR sensor is guaranteed. Accordingly, the majority of published snow cover studies relying on SAR data are based on C-band sensors, with X- and L-band following on second and third position, respectively (see Figure 3 for a detailed overview).

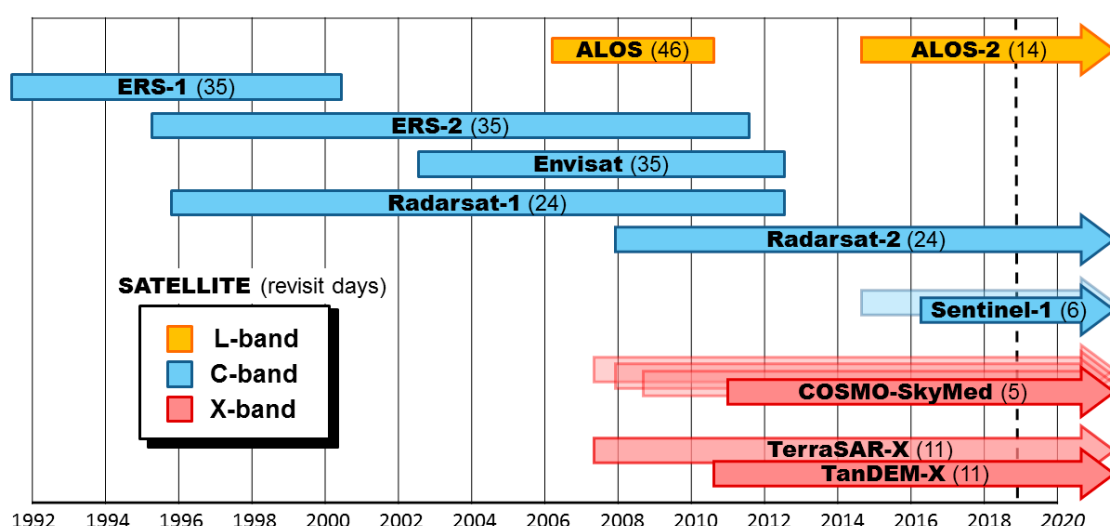


Figure 2. The operating periods of available satellites equipped with SAR sensors and their band as well as revisit time configurations (number in brackets referring to the revisit time in days). L-, C-, and X-band SAR refers to frequency of 1–2 GHz, 4–8 GHz, and 8–12 GHz; wavelength of 30–15 cm, 7.5–3.75 cm, and 3.75–2.5 cm, respectively [62].

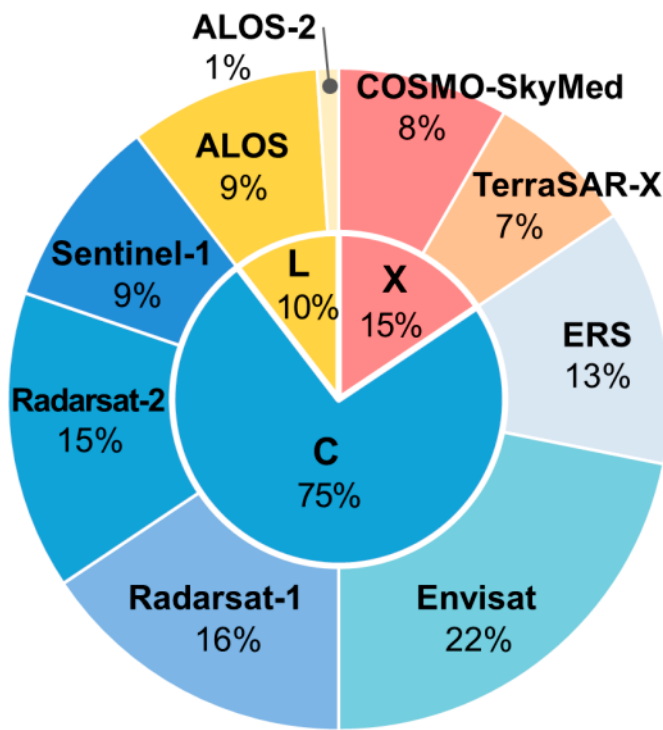


Figure 3. The frequency of different SAR sensors/bands being employed for snow cover studies.

Due to the longer wavelength of L-band SAR and the subsequently deeper penetration of the L-band signal into the snowpack, the snowpack remains nearly invisible in the L-band data [124]. Therefore, studies about the implementation of L-band data to analyze snow cover properties are scarce although it has a longer history than X-band SAR. X-band SAR has been facilitated more often than L-band, which is due to the higher sensitivity of the X-band signal to the snowpack even when compared to C-band [115,125]. Moreover, multi-satellite constellations are available such as COSMO-SkyMed operated by the Italian Space Agency (ASI) and the TerraSAR-TanDEM-X twin satellite employed by Airbus Defense and Space and the German Aerospace Center (DLR).

3.2. Spatial and Temporal Scale of Snow Cover Studies

Snow covers extensive areas around the globe, including high altitudes featuring complex terrain, high latitudes, and boreal forests. It is important to get an overview of the study regions of the already conducted research. Additionally, some studies focus specifically on a certain land cover while excluding others (e.g., focusing on glaciers or masking out any forested areas). In order to identify possible research gaps or areas where SAR-based snow cover analyses are still facing major challenges, every study incorporated in this review was evaluated by its location and land cover characteristics. Figure 4 presents the result of this evaluation, breaking the study regions down into study regions' types (Figure 4a), study mountainous regions (Figure 4b), and the distribution of study regions inside the European Alps (Figure 4c). The map presented in Figure 4d visualizes the locations of the studies and the frequency with which these regions have been investigated so far.

It can be observed that the majority of studies were conducted in mountainous regions, which is reasonable as these regions are frequently affected by cloud coverage so the advantage of SAR can be demonstrated. However, the relatively small number of studies conducted in forest and glacier areas was also noted although snow commonly exists in these region types. This finding suggested that the current SAR-based SCE detection studies still have further investigation potential in these regions. Regarding the hotspots of the frequently studied areas, Asian and European mountain ranges represent around 85% of available study regions, as also shown in Figure 4d. The European Alps have been studied most intensively (32%), followed by Himalaya (31%). Within the European Alps,

most studies have been conducted in Italy and France (Figure 4c). Other global mountain ranges like the Andes, Caucasus, Rocky Mountains, or Ural have merely been investigated. Within the polar regions, several studies exist for Greenland and Antarctica, where the interaction between snow cover and glaciers has been investigated. The imbalance of study areas also indicates that more research is necessary in these areas.

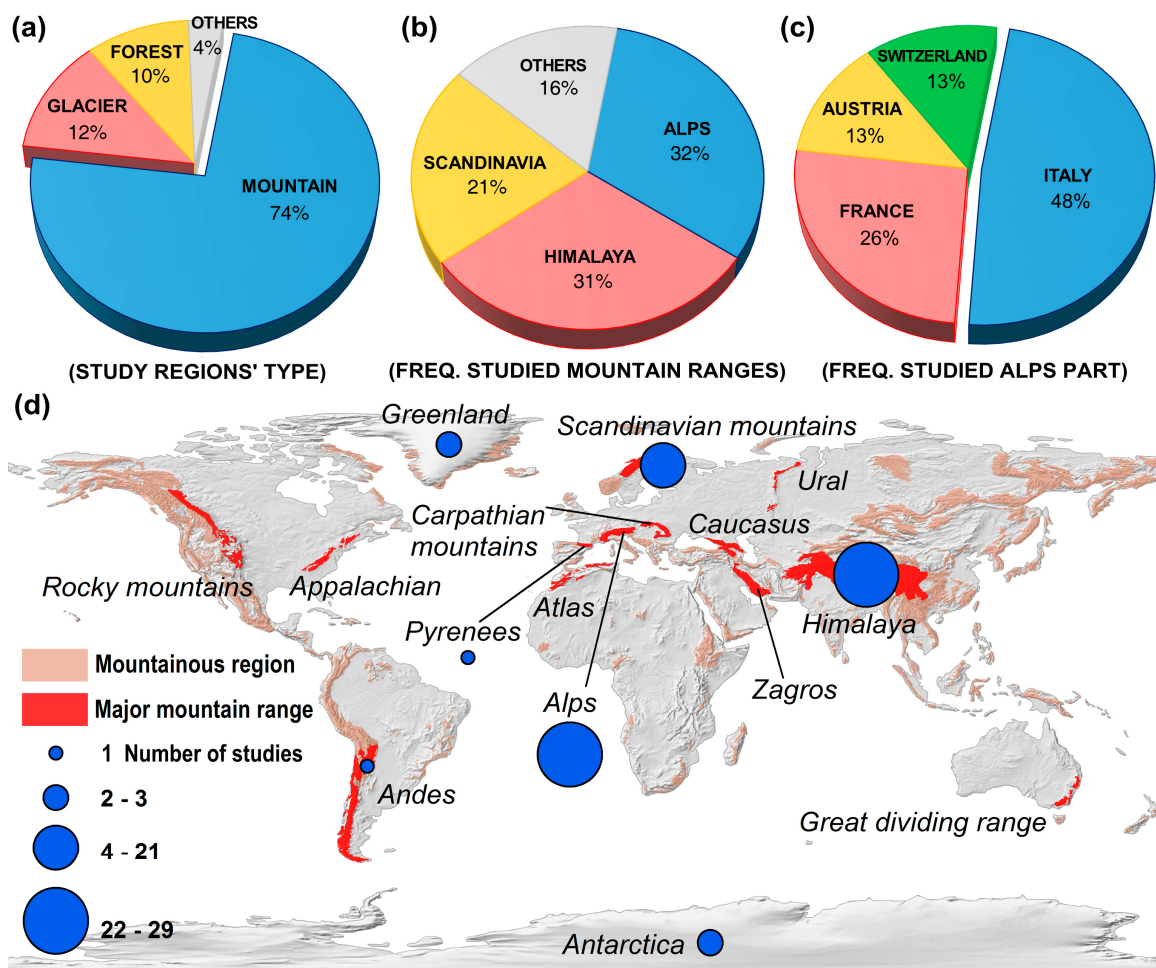


Figure 4. Overview of published SAR-based snow cover studies. (a) Study regions' type; (b) frequency of studied mountain ranges; (c) distribution among countries within the Alps; (d) geographic overview of performed studies.

Not only the location but also the spatial extent of the study regions is important as it can help assess the maturity and readiness of algorithms. Figure 5a illustrates the size of the study regions. Most of the studies were conducted on a local scale as visible in Figure 5a. These studies are usually limited to a specific test site, which in more than 50% of the cases is smaller than 2500 km^2 . Only five studies investigated areas greater than $200,000 \text{ km}^2$ (the size of Alps is around $298,128 \text{ km}^2$). One motivation for these relatively small study sites is the spatial extent of typical SAR-data footprints itself. Many studies were designed to be conducted only within the boundary of a single SAR-footprint, which limits their extent according to the coverage of the respective SAR-mission.

When trying to evaluate the transferability of a study, not only the spatial extent is of interest, but also the amount of observations included. This information helps assess whether a proposed algorithm can work under different weather and snowpack conditions. The number of sensed years and the average number of observations conducted per sensed year is illustrated in Figure 5b,c, respectively. It must be noted that, even for studies we categorized as multi-year monitoring in Figure 5b, none of

them provide a consistent time-series of SCE result but only few random observations in each observation year. Hence, we further investigated how many observations were utilized on average for each year and study, and illustrated these findings in Figure 5c. Based on Figure 5b,c, it can be found that more than half of the published studies investigated snow cover for one year with an average of two observations within this year to account for the dynamics of the snowpack (see Figure 5b,c). These sparse observations indicate that current studies are still immature compared to the conventional optical-based SCE monitoring approach.

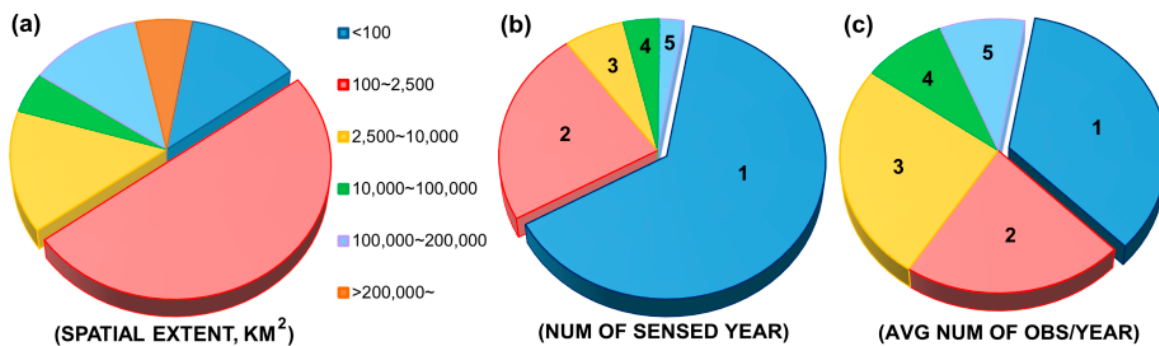


Figure 5. Spatial and temporal overview of published SAR-based snow cover extent (SCE) detection studies. (a) The spatial extent of studies; (b) number of sensed years; (c) average number of observations per sensed year. Note that none of the studies categorized as multi-year monitoring in (b) provide a time-series of SCE results, but only few random observations for each year. Thus the average observations conducted per sensed year of each study are illustrated in (c).

3.3. Employed Methods to Monitor Snow Cover with SAR Data

As the development of SAR sensors and image processing techniques progresses, the sensing target of snow also changes. For the following discussion, we defined three different sensing targets of snowpack: Wet SCE, total SCE, as well as wet and dry SCE. Here we must address the difference between wet and dry SCE as well as total SCE, although the overall SCE can be retrieved by both strategies, only the former can discriminate wet and dry SCE, respectively. Namely, wet and dry SCE sensing strategies can provide more information than a total SCE approach.

3.3.1. Wet SCE Detection

The most commonly used approach to derive the extent of wet snow cover is by exploiting the backscatter coefficient. As outlined in Section 2.2, the backscatter coefficient drops significantly when a snowpack starts to melt, therefore containing liquid water, which decreases the dielectric constant.

The first algorithm to exploit this behavior was published by Rott and Nagler in 1995 and 2000 [126,127]. They relied on two SAR images (one is sensed during the snow-covered period σ_{ws}^0 , and the other is a reference image σ_{ref}^0 which is sensed in either the snow-free or the dry-snow period) featuring the same imaging geometry (i.e., repeat pass pair) as well as a digital elevation model (DEM). The main workflow comprises pre-processing and wet snow mapping as illustrated in Figure 6. For pre-processing, the two images are calibrated, coregistered, multilooked, speckle-filtered, the scattering coefficient is transformed to a logarithmic scale (dB), the ratio between the two observations is calculated (see Equation (1)), and finally the result is geocoded. The geocoding is based on the DEM and produces a SAR layover mask, a shadow mask, and a LIA map. After pre-processing, the geocoded ratio map is classified based on a threshold to derive the binary wet snow extent. A threshold of -3 dB has proven to be robust enough to achieve satisfactory results, and was used in many subsequent studies.

$$\frac{\sigma_{ws}^0}{\sigma_{ref}^0} < -3 \text{ dB, wet snow} \quad (1)$$

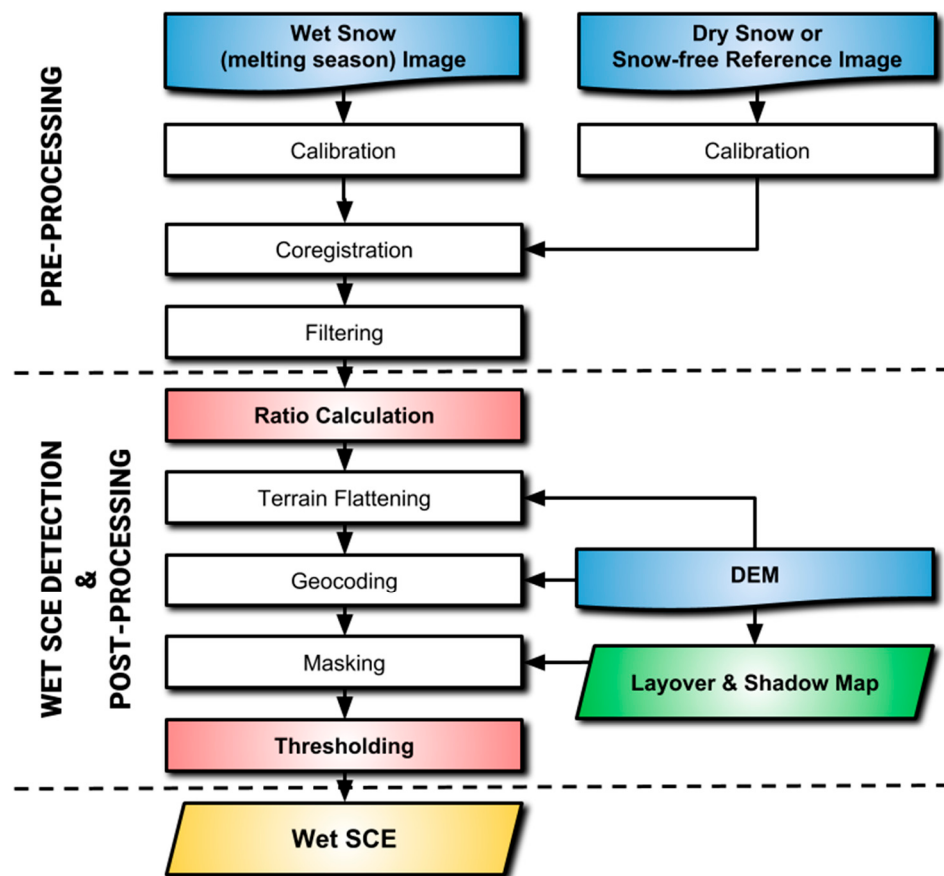


Figure 6. The overall workflow of the backscattering-based algorithm to detect wet snow.

As this method is easy to implement, it was applied successfully to most SAR sensors and study regions. Consequently, the backscattering coefficient-based method is known as “Nagler’s method”. Yet, this method uses only a single equation with a fixed threshold to retrieve the binary result; this result, however, is limited as the random noise of SAR would inevitably degrade the single image as mentioned in Section 2.1 and the binary snow results do not meet the real condition. Several improvements have therefore been achieved for “Nagler’s method”:

- Mapping of snow cover fraction

Binary snow cover products (i.e., a pixel is flagged as either snow covered or snow free) contain uncertainties especially along the transition between snow covered and snow free areas. Traditionally, a pixel containing more than 50% of snow cover would be considered fully snow covered in a binary product [128–130]. Thus, an approach to derive fractional snow cover information from SAR-data is required. Therefore, Malnes and Guneriussen [131] utilized a sigmoid-function based on the assumption that each pixel is a mixture of dry snow, wet snow and snow-free surface. This approach was later refined into different forms [132,133].

- Refined reference image selection

Selecting a suitable image for representing the snow-free (or dry-snow) ground surface backscattering conditions is critical, as the ratio between this reference image and the observation containing the wet snow accounts for the accuracy of the wet snow detection. It is important to ensure that the reference image selection is selected carefully. Since Nagler’s first publication [126], soil moisture has been frequently proven to bias single reference images [134,135]. Thus, Pettinato et al. [136] suggested reference scenes acquired under dry snow conditions recorded during wintertime.

Another approach is using the average of several images originating from a similar sensing period [137]. However, the temporal distance between reference images has to be taken into account, ensuring that longer intervals between observations do not introduce additional uncertainties [121]. Koskinen et al. [138] selected one image observed during the melting period σ_i^0 and two reference images (one acquired at the beginning of melting period σ_w^0 , and another acquired after melting period σ_g^0) to estimate the snow-free ground F_g :

$$F_g = 100 \times \frac{\sigma_i^0 - \sigma_w^0}{\sigma_g^0 - \sigma_w^0} \% \quad (2)$$

Luoju et al. [139] used the same formula in an approach proposed as the linear interpolation phase step. They applied the algorithm not pixel-based but at a bigger scale to eliminate the influence of SAR speckles. They also tested the usability of multi-year reference images; they concluded that the reference image does not necessarily need to be sensed in the same year as the classified melting season. Namely, a reference image from the past may be used to estimate future snow cover conditions.

Thanks to these improvements, “Nagler’s method” has remained the most commonly applied algorithm in the past 20 years. As numerous new satellites with different wavelength designs have been launched since “Nagler’s method” was published in 2000, the -3 dB threshold value for the ratio map segmentation has also been customized for different sensors and locations [121,125,140–143]. However, as this approach cannot be applied to L-band SAR (because the backscattering values from the snow-covered scene and the reference scene containing no or dry snow are similar [144]) and can only detect wet SCE, other SAR-based algorithms have been explored as well.

3.3.2. Total SCE Detection

Based on the phase information of two SAR images recorded for the same location but at different observation times, the similarity of surface conditions (coherence) can be revealed based on interferometric SAR (InSAR) technique. The underlying theory of InSAR-based total snow detection is that, in comparison to snow-covered areas, the snow-free area can preserve a high coherence between two sensed dates. The reason for the decorrelation between snow-covered observations (in both dry and wet snow) is the alteration of the SAR penetrating depth and the scattering mechanism [106,145]. Hence, in contrast to the backscattering-based approach presented in Section 3.3.1 that can only detect wet SCE, the InSAR-based approach can detect both wet and dry snow.

The first attempt of using repeat-pass InSAR techniques was conducted by Shi et al. [146], utilizing space shuttle-based SIR-C images to create coherence maps. Later, Strozzi et al. [147] pursued this approach, applying it to ERS images; they found that the coherence helps distinguish the SCE better than conventional backscattering-based methods. Guo et al. [148] employed two pairs of InSAR observations sensed before and after a snowfall event, and classified the total SCE with coherence thresholds. Wang et al. [144] proposed a more elaborate workflow to track the total SCE change in different periods. First, they used the normalized difference snow index (NDSI) derived from optical images as well as land cover information to initially estimate the tree and snow line elevation. Additionally, temperature information was incorporated to decide the actual snow condition. Finally, they applied a coherence threshold to derive the type of surface and snow cover change. Figure 7 illustrates the general workflow of InSAR-based algorithms to detect total snow cover.

The definition of an appropriate coherence threshold for the snow cover classification is critical. Wang et al. [144] utilized an NDSI-based snow cover classification result to determine final coherence threshold for each area. However, using a hard threshold to classify snow cover may lead to misclassification, since the coherence values of snow-covered and snow-free areas largely overlap [149]. To the authors’ knowledge, this problem has not been addressed in any study so far.

Another challenge for InSAR-based snow cover detection is the influence of various additional factors on the coherence value. According to Zebker and Villasenor [150], temporal, spatial and thermal

factors influence the coherence value. Essentially, He et al. [149] discovered that the coherence value is related to the polarization mode, land cover type, and LIA. Those factors need to be considered to improve the reliability of InSAR-based snow detection approaches.

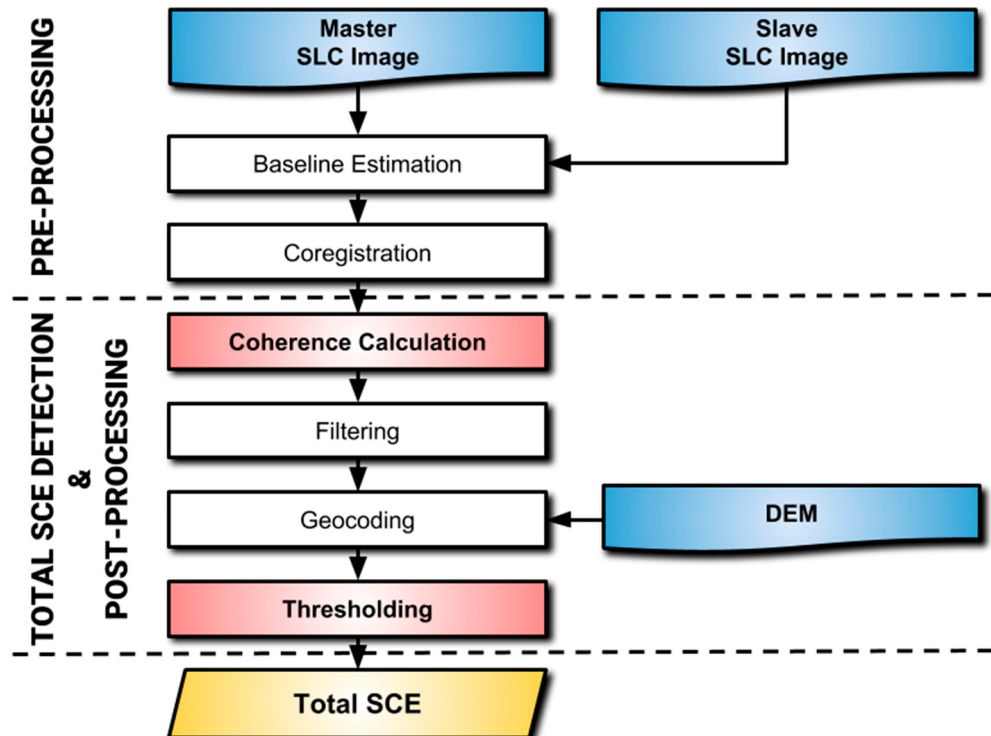


Figure 7. The overall workflow of interferometric SAR (InSAR)-based algorithms to detect total snow cover. Master and slave image refer to the two single look complex (SLC) SAR images used to generate an InSAR pair.

3.3.3. Wet and Dry SCE Detection

Initially, when polarimetric SAR (PolSAR) techniques were still immature, it was concluded that SAR is unable to detect dry snow [33,68,151]. Nevertheless, as dry snow detection is crucial for applications like SWE estimation or other hydrological applications, empirical or topographical rules were applied to predict the dry snow based on the wet snow extent. Nagler and Rott [126] presumed regions with elevations higher than the extent of the wet snow were dry snow. This method was modified [131,152,153] and further improved by including measurements of air temperature [151,154]. Another approach is based on presumption of snow status change with time as shown in Pettinato et al. [155] and Brogioni et al. [156].

However, those wet snow based approaches to estimate the dry snow extent have proven inaccurate. Studies following Malnes's method to derive dry SCE found large overestimations [33,68]. In addition, Storvold and Malnes [154] stated their algorithm could face problems in early spring when dry snow extent could be extensive while wet snow still being absent. Moreover, these approaches do not account for the influence of wind to redistribute snow [154]. Consequently, an alternative approach, i.e., PolSAR technique, was explored to detect wet and dry SCE directly from SAR imagery.

Rott [157] proposed a depolarization approach, i.e., calculating the ratio of cross- and co-polarization of airborne AIRSAR; Shi and Dozier [158] used SIR-C/X-SAR to test multi-frequency and multi-polarization. Early spaceborne SAR sensors; however, were generally only equipped with single polarization ability, such as ERS-1/2 (VV) and Radarsat-1 (HH). Dual polarization mode became available after the launch of ENVISAT-ASAR in 2002, offering new possibilities to explore the potential of multi-polarization repeat-pass methods for snow cover mapping.

The key of PolSAR-based wet and dry snow cover detection is to extract the geometrical scattering characteristics of ground features by decomposing the received SAR signal. The backscatter from each ground feature is composed by various unique signal-feature interactions; PolSAR decomposition therefore offers the possibility to reveal how a particular surface feature reflects the incoming SAR signal and what physical characteristics that feature might have. For instance, the frozen forest canopy leads to high correlation of the polarization due to surface backscattering during wintertime, while low correlation results from the snow-covered ground surface. Once the snow becomes wet, the polarization correlates again [159].

The development of PolSAR techniques led to numerous decomposition methods to derive PolSAR parameters. The most commonly employed decomposition parameters include Pauli decomposition [160] and H/A/ $\bar{\alpha}$ [160]. They decompose the coherence matrix in different ways and thus form different parameters, such as former's single/odd, double/even bounce and volume scattering. The H/A/ $\bar{\alpha}$ decomposition can even reveal the scattering angle and degree of randomness of the sensed target. For detail decomposition theory and examples can refer to [161,162]. However, as there are countless decomposition indexes, selecting the most feasible parameter is challenging. He et al. [163] calculated the Jeffreys—Matusita (J—M) distances [164] to filter feasible parameters for distinguishing dry and wet snow. Huang et al. [165] plotted the normalized value of each parameter of each land cover type to observe their overlap. The parameters showing fewer overlapping of dry and wet snow were chosen.

Due to the various information (referring to Appendix A) that can be retrieved from PolSAR parameters, more details about the characteristics of snow cover can be obtained when compared to backscattering- or InSAR-based approaches. For instance, Baghdadi et al. [166] revealed that backscattering of wet snow is primarily caused by surface scattering; Shi and Dozier [92] found that snow wetness is proportional to surface scattering and inversely proportional to volume scattering. In addition, the morphology of snow also influences the scattering, such that an older snowpack would have larger grain size and thus would lead to increased volume scattering [30]. Singh et al. [30] found that snow-covered regions show lower entropy, H(1-A) as well as higher polarimetric anisotropy; thus they proposed a threshold method to detect snow cover, which resulted in an accuracy comparable to a supervised Wishart classification. Reppucci et al. [167] observed that dry snow is characterized by higher values in the Pauli surface parameter and lower value in the double-bounce parameter. Therefore, a combination of the two parameters enables to calculate the difference and then to map dry snow cover. Based on the observation that dry snow shows lower H and $\bar{\alpha}$ values, they also derived the ratio of H and $\bar{\alpha}$ to detect dry snow. Similar techniques were employed by [96,118,159,168,169], calculating the difference of available parameters or relying on machine learning (ML) classifications to detect snow cover. Venkataraman et al. [170,171] even proposed a Radar Snow Index (RSI) to estimate the total SCE based on polarization fraction parameters. To deal with the influence of underlying land cover types, Martini et al. [172] suggested an advanced supervised polarimetric contrast variation enhancement (PCVE) to enlarge the contrast of dry snow.

Based on the research from recent years it became obvious that PolSAR-based detection of snow cover is developing quickly and that there is still potential to improve and complement existing approaches. Figure 8 presents an overview of the three different mainstreams of PolSAR-based wet and dry snow cover detection algorithms.

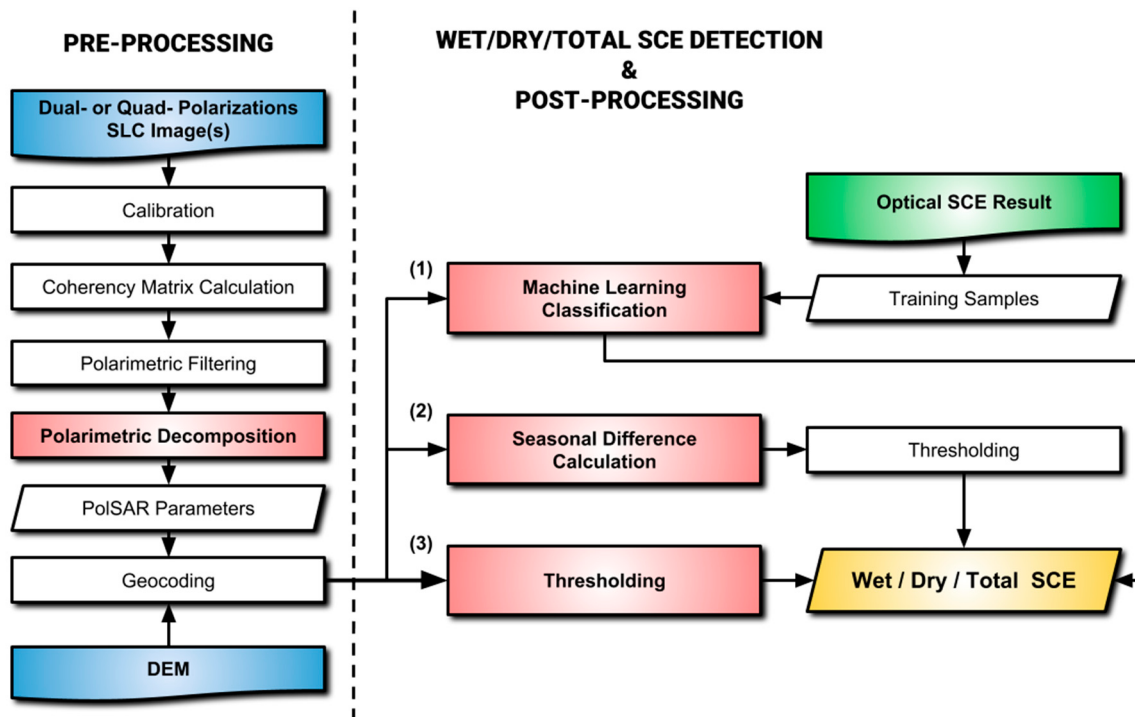


Figure 8. The overall workflow of polarimetric SAR (PolSAR)-based algorithms to detect wet and dry snow cover, including (1) machine learning classification trained by external SCE result; (2) the calculation of seasonal parameters' difference before thresholding, and (3) the direct thresholding.

3.4. Algorithms Utilized to Investigate the Different Snow Cover Types

After reviewing the advancements in detecting snow cover from SAR data within the last three decades, a comprehensive overview of the different mapping approaches for different snow cover types that can be observed relying on these approaches emerged, which is presented in Figure 9. When analyzing the snow type, the review revealed that more than half of the available studies focused on the retrieval of wet snow only, while 30% of the studies aimed at both, wet and dry snow (Figure 9a). Less than 16% of the studies were designed to retrieve total SCE or dry snow only. This mismatch does not indicate that dry snow is less important than wet snow but it clearly shows that the detection of dry snow from SAR-data is still challenging.

The different approaches to detect wet, dry, and total SCE (Figure 9a) can further be divided: For wet snow (Figure 9b), 82% of studies employed “Nagler’s method”, while InSAR- and PolSAR-based approaches account for 7% and 10%, respectively. Regarding dry snow (Figure 9c), more than 60% of the studies relied on topographic empirical determination, which is an approach frequently employed together with “Nagler’s method” (see Section 3.3.3). Another 21% and 10% of the studies utilized PolSAR (including PCVE) and InSAR techniques, respectively. The remaining 7% of the studies applied logic conditional rules to identify dry snow extent. When it comes to the detection of total SCE, (Figure 9d), 77% of the reviewed studies relied on PolSAR while only 23% applied InSAR techniques. In summary, when reviewing Figure 9, the predominance of PolSAR and InSAR for dry and total snow cover detection becomes obvious, while backscattering-based approaches are clearly the methods of choice to detect wet snow.

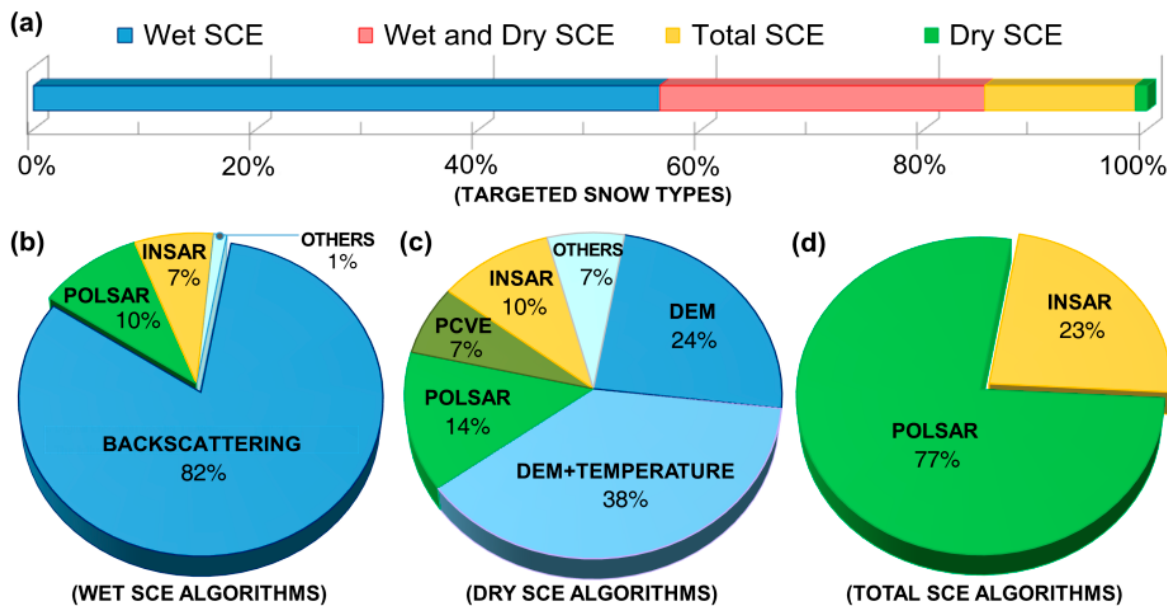


Figure 9. Overview of targeted snow types and corresponding algorithms. (a) Targeted snow types and employed algorithms for (b) wet (c) dry (d) total snow cover extent (SCE).

Machine Learning Classification Methods for Advanced SAR Information Analysis

Additionally to the aforementioned algorithms, ML is commonly performed on advanced SAR-derived information especially derived from PolSAR-based approaches. Because SAR images can contain a considerable amount of noise, the derived PolSAR parameters are often challenging to be manually extracted. As PolSAR-based approaches are a comparatively new technique, the number of studies employing ML classification is small (only 19%). Owing to the maturity of optical-based snow cover monitoring techniques and products, training samples for supervised algorithms are available. Thus, supervised algorithms are slightly more common than unsupervised approaches.

The most commonly employed supervised ML classification approach is the support vector machine (SVM), which is well known for its ability to solve high-dimensional non-linear classifications with only small samples [173]. Compared to maximum likelihood and decision tree methods, SVM produced higher snow cover classification accuracies [165] and thus was utilized for both InSAR-based [149,163] and PolSAR-based studies [165,174]. However, random forest (RF) also attracts attention for its simplicity and low computation load [143].

3.5. Quality Assessment Methods for SAR-Based Snow Cover Products

In the present SAR-based mainstream algorithms, there is no straightforward method to directly generate reliability indices to allow self-validation as in other SAR-based cryospheric studies such as the signal-to-ratio value of pixel-offsets for glacier velocity tracking [75]. Thus, several studies focused on quality indicators for assessing the reliability of a snow cover products. Malnes et al. [151] and Solberg et al. [33] utilized a confidence flag denoting the probability for a correct classification; Schellenberger et al. [134] introduced the probability of error (POE) to evaluate each pixel's classification reliability. Practically, validating SAR-based snow cover products using external, independent data is preferable. Overall, around half of the reviewed studies utilized snow cover products derived from spaceborne optical sensors as ground truth, with Landsat and MODIS accounting for most of the employed sensors (Figure 10). AVNIR-2 is used for validating PALSAR-based studies, as both sensors are mounted on the same satellite platform. Sentinel-2 is usually used for comparisons with Sentinel-1 results; Gaofen-1 (GF-1) is often utilized for validating studies in mainland China. Airborne and ground-based data account for a much smaller portion of validation approaches owing to the relatively high costs and

limited spatial coverage. The fact that ~40% of the reviewed studies did not include any validation at all indicates that many of the published SAR-based snow detection techniques are in an early stage of their development.

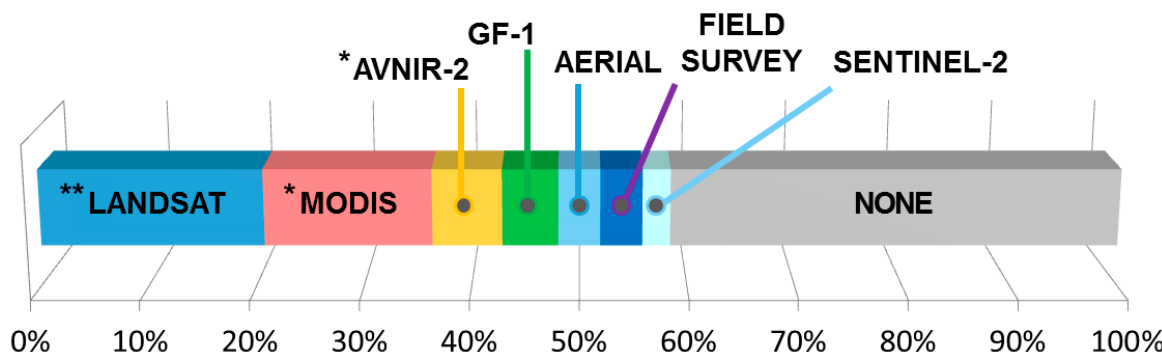


Figure 10. External/Ground truth data used for validating SAR-based snow cover products. * Advanced visible and near infrared radiometer type 2 (AVNIR-2) sensor onboard on Advanced land observation satellite (ALOS) satellite; moderate resolution imaging spectroradiometer (MODIS) sensor onboard on Terra and Aqua satellites; ** Landsat-series missions compose different optical sensors.

In addition to conventional confusion matrix-based accuracy evaluations, Luoju et al. [139,175] proposed a quantitative analysis approach based on the RMSE to check the improvement made by each refining algorithm; Reppucci et al. [167] compared the resultant SCE with an elevation map to check whether the distribution of snow is reasonable.

4. Critical Auxiliary Data Necessary to Support Detecting SCE from SAR Data

In addition to the sensor types and algorithms, other critical and commonly employed datasets help improve the accuracy of the obtained snow cover classification, including DEM, land cover maps and meteorological information. As shown in Figure 1, these parameters directly affect snow cover distribution and condition, and it is therefore advisable to include these auxiliary datasets to the workflow. They may not be necessary to operate the SAR-based snow cover detection; they, however, can improve the quality of the results.

4.1. Digital Elevation Model, Influence of Topography on SAR-Based Snow Detection

The influence of the topography on SAR-based snow cover detection is evident, as snow cover distribution is directly linked to elevation, aspect (facing direction of topography), and slope of the study region. Moreover, local topography affects the LIA, which largely affects the quality of SAR image pre-processing and final results.

Elevation plays a significant role in snow cover distribution. Algorithms like the wet snow-dependent dry snow detection relies on the spatial relationship between wet and dry snow cover extent and elevation (see Section 3.3.3). Haefner [176] analyzed the seasonal difference of backscattering coefficients in various elevation zones and found larger differences in higher altitudes. Tsai et al. [143] also found the importance of elevation is crucial for total snow cover mapping. Aspect and slope are also critical for not only how snow is distributed but also how SAR can sense the snow. Li et al. [177] compared the snow line altitude for several regions and discovered that glaciers facing south have higher snowline altitudes, which is caused by more intense solar radiation on south facing slopes. Park et al. [169] identified that the seasonal difference between H and α is more pronounced for front-slope (the slope facing the sensor).

Topography not only affects snow distribution, it also affects the SAR signal viability. Based on the DEM a shadow and layover map of SAR can be generated. Steeper topography or regions closer to the nadir of the sensor would naturally lead to more SAR shadow and layover regions [65],

where useful ground information is blocked or degraded. Hence, almost all studies calculated the mask during the geocoding step and later re-used it to mask out the results, as illustrated in Figure 6. However, these terrain-induced radiometric effects and the local illuminated brightness should be mitigated by adding a terrain correction based on DEM as well as the acquisition geometry of SAR [178].

Moreover, for the backscattering-based approach, the influence of LIA on the SAR signal was already identified in Nagler's first research [126], and confirmed by many subsequent studies [86,103,121,141,179]. The backscattering of wet snow is more susceptible to the variability of LIA than dry snow because the backscatter of the latter is mainly reflected from the snow/ground interface, as modeled by Malnes and Guneriussen [131]. Nagler et al. [140] found the backscattering from snow can decrease even more for a very high LIA, which reduces the difference between wet and dry snow. This angle-dependency influences the accuracy of backscattering-based thresholding approaches, especially for wide-swath SAR images such as ASAR and Radarsat [96,154]. It was also suggested that the LIA difference between the reference and the observed image should not exceed 10° [175]. The range direction resolution would also decrease dramatically in low LIA, and the signal-to-noise ratio for low reflective surfaces decreases in high LIA [140]. Therefore, areas with extreme LIA values should be masked out by setting LIA limitations [126,127,134,140].

The influences of LIA on both InSAR-based and PolSAR-based approaches are also significant. He et al. [149] found the coherence value increases from 0° to 30° LIA and decreases from 30° to 90° LIA. Dedieu et al. [35] found that when the LIA is less than 35° , the dominant scattering mechanism changes from volume to single-bounce scattering. Park et al. [169] revealed that the change of H and α caused by the snowpack would be smaller for lower LIA. Usami et al. [180] observed that the degree of polarization decreases when the LIA increases. Furthermore, several studies found that the impact of surface roughness on the signal is more significant for high LIA [94,181].

4.2. The Influence of Land Cover (Vegetation) on Snow Detection from SAR-Data

Another factor affecting SAR-based snow cover detection is land cover. This effect was first described by Koskinen et al. [138] when they analyzed the backscattering coefficient values of different surface conditions depending on different types of land cover. Results clearly showed that the presence of vegetation significantly decreases the backscattering difference between wet snow and dry snow as well as bare ground. Schellenberger et al. [134] also reported that snow-covered and snow-free areas in forest regions are difficult to discriminate as the backscatter is significantly influenced by canopy [182].

According to the model proposed by Pulliainen [183], SAR backscattering relates to the transmissivity of a forest canopy, which is influenced by stem volume. The different scattering coefficient levels of grassland, crop field and dense forest confirm these results [121,134]. Duguay and Bernier [184] found that backscattering coefficient is continuously increasing with increasing vegetation height. Therefore, applying only one fixed backscatter threshold to classify snow cover in a region with varying land cover may lead to inaccurate results [121]. Additionally, results from polarimetric models indicate that backscatter of dry snow is strongly sensitive to the underlying surface as the backscattering originates from the snow/ground surface interface [169,172]. He et al. [163] concluded that stems of snowcapped shrubs and grass lead to higher volume scattering for dry snow than for wet snow. Dedieu et al. [35] reported difficulties detecting snow cover in forested areas as the tree structure affects the scattering of the SAR signal (double-bounce with tree trunks, volume scattering with foliage and single scattering with forest floor). The seasonal phenology of trees (leaf fall before winter) also alters the scattering behavior. Park et al. [169] concluded that the presence of woodlands could increase volume scattering as well as H and α .

Forest also affects InSAR-based approaches. The coherence values of InSAR are found to be commonly lower in densely vegetated regions [149,163]. Thakur et al. [102] concluded that this reduction in coherence is connected to both snow cover and the presence of forests. Kumar and Venkataraman [185] reported that the random motion of leaves due to wind would reduce the coherence significantly.

Aforementioned studies intensively indicate that vegetation would limit the accuracy of SAR-based snow detection approaches; however, based on previous studies there is no decisive threshold for any vegetation index such as biomass or canopy closure. As a result, many studies use masks to eliminate the influence of densely forested regions. Rott and Nagler [126,127] as well as Notarnicola et al. [186] masked the agriculture areas. Practically, external land cover products [149,163,175,186] or land cover maps generated during the pre-processing workflow [35,102,144,187] may serve as masks. Masking of critical land cover regions; however, may reduce the size of the study region considerably. Therefore, Schellenberger et al. [134] divided the backscattering ratio map for each land cover and calculated the geometric mean for each class as its threshold; Tsai et al. [143] built the model for each land cover type and mapped total SCE individually.

4.3. Utilization of Temperature and the Need for Snow Record Data

Although most SAR-based algorithms such as “Nagler’s method” [126] did not require ground information as an input, meteorological data about temperature and precipitation makes estimating the snow cover conditions easier. For example, it is possible to infer the retreat of snow between two observations if the daily mean air temperature is rising [133] and the existence of wet snow can be postulated when surface temperature is observed to be near 0 °C [68]. Thus, many studies included temperature information gathered by ground surveying or meteorological stations [30,118,136,149,163,169,188].

However, the often sparsely distributed meteorological stations hardly satisfy the required spatial resolution necessary to derive an areal inventory of surface temperatures. Hence, Malnes et al. [151] calculated a temperature map by interpolating the data derived from meteorological station network. Another approach is utilizing spaceborne thermal imagery. Salcedo and Cogliati [85] used atmospheric profiles of temperature and water vapor at the sensed time to derive the surface temperature based on recorded satellite radiance. Moreover, snow record data also helps to analyze the snow cover conditions. Luojus et al. [189] utilized the snow accumulation recorded by snow stations to decide when the snowmelt period ended.

5. Discussion

The studies investigated in this review show that SAR-based methods to detect and characterize snow cover have been developing rapidly and profoundly within the last three decades. This development includes the design of new spaceborne SAR sensors, new algorithms to detect snow, higher spatial and temporal resolutions of the derived products, increasing accuracy, and a deeper understanding of the underlying processes. The developments identified will be discussed in more detail in the following sections.

5.1. The Development of Spaceborne SAR Sensor Design

The development of SAR sensors advanced remarkably within the last 25 years in terms of instrument design, temporal and spatial coverage, and data distribution policy. Band design was limited to C-band, but has been extended to X-band, as shown in Figure 2. This offers new opportunities to detect and monitor snow cover, because the capabilities of X-band SAR to detect snow are superior to C-band, as outlined in Section 3.2. Moreover, study suggested that Ku-band SAR may be most suitable to detect snow cover as it can detect even shallow and dry snow [87], which was planned (but not realized) for ESA’s 7th Earth Explorer mission candidate, Cold Region Hydrology High-resolution Observatory (CoReH₂O) satellite, meant to be equipped with X- and Ku-band SAR sensors [190].

Furthermore, the capabilities to detect snow relying on different polarizations attracted more attention. Among all snow cover detecting studies based on polarimetric information, almost all employed SAR images in full-polarimetry mode including PALSAR-1 [30,163,169,170] and Radarsat-2 [35,165,167,168,191]. Early airborne SAR and recent spaceborne studies already suggested that multi-polarization SAR—and especially fully polarimetric SAR—is more suitable to detect snow

and ice than single/dual-polarization [102,191,192]. Possible reasons are that multi-polarimetric SAR has a higher sensitivity to the state of snow [35] and that it can greatly eliminate the topographic distortion [30].

Shortening the revisit time is another advantage of contemporary SAR missions. Practically, the time difference between two repeat-pass SAR images is the most important factor for InSAR-based approaches. Researchers have confirmed that the coherence of InSAR within snow-covered areas would decrease dramatically if the temporal difference is more than one month [142]. In addition, if the revisit time is too long, more than one melting/snow fall event may have occurred in the meantime [144]. In this regard, the value of the COSMO-SkyMed (CSK) constellation is remarkable. Thanks to their orbit design, four satellites (CSK1-4) significantly shorten the revisit time and thus largely eliminate temporal decorrelation [193,194], which provides a potential to map SCE with a much higher temporal resolution [187].

The wider swath coverage of contemporary SAR sensors allows snow monitoring in larger spatial scales, which may also reduce costs. Nagler and Rott [195] proved that all sensing modes of ASAR images are suitable for processing “Nagler’s method”. Although the definition of wide swath mode varies for different sensors (e.g., ASAR’s 150 or 500 km, Radarsat’s 300 or 500 km, PALSAR’s 250 or 350 km, and Sentinel-1’s 250 km), it is clear that they are more efficient than traditional sensing modes providing swath widths below 100 km.

In addition to sensor’s hardware design, another important milestone is the free data policy of ESA. Before Sentinel-1, no long-term, openly accessible SAR datasets were available, which stands in contrast to the free of charge archives of optical sensors such as Landsat and MODIS. As a result, until recently the cost of spaceborne SAR data was much higher compared to optical imagery [68], which inevitably limited the operational use of SAR-based snow cover detection or the subsequent possibility of merging SAR and optical snow cover products.

5.2. The Advances of SCE-Detection by SAR

Conventional backscattering-based approaches were subject to criticism for using a hard threshold to classify snow cover, as numerous factors may affect the backscattering value. For instance, in a warm winter more frequent melting/refreezing cycles would lead to bigger grain sizes and thus influencing the backscattering coefficient [196]; sudden changes of air temperature or heavy snowfall events may cause snow metamorphism, altering the snowpack conditions [188]. Variations of soil moisture may also disturb the backscattering coefficient values [197]. Moreover, the geometry of two images needs to be identical to preserve similar LIAs [197]. If thresholds are set too low/high, the final SCE would be under/overestimated. However, backscattering-based algorithms also show one great advantage, i.e., they do not require training samples for classification. This fact avoids the manual selection of a classifier and saves time for the classification, which is an asset for an automated processing over longer periods or large regions.

In contrast to backscattering-based approaches, PolSAR-based algorithms have the merit of less LIA dependency. Hence, theoretically they are more suitable for mountainous terrain. Another benefit is the availability of additional information such as scattering angle and degree of randomness inherent to the polarimetric data. Furthermore, PolSAR technique only requires one image, which increases the sensing frequency and real-time monitoring capabilities. The different ways to decompose the covariance matrix, however, results in countless derived parameters; a suitable selection of included parameters and a proper filtering of redundant data therefore is critical. Moreover, the process of decomposition is more time-consuming when compared to backscattering-based approaches as it involves more matrix calculations.

InSAR-based algorithms are supported by the maturity of available InSAR processing software. The main challenge is the revisit interval of the SAR sensor and the sometimes rapid change of snow cover conditions (depending on location, weather conditions, and season). Nevertheless, it can be postulated that InSAR-based approaches may become more promising in the near future, as the revisit

time of SAR sensors has enhanced significantly. Overall, the comparison of mainstream SAR-based approaches is shown in Table 3, which provides guidance for choosing the appropriate algorithm based on the targeted snow cover type and SAR image availability.

Table 3. Overall comparison of the three mainstream SAR-based snow cover detection approaches.

Detection Approach	Backscattering-Based	InSAR-Based	PolSAR-Based
Background theory	The backscattering coefficient reduces when snow becomes wet	Coherence loss over snow covered surfaces	Scattering mechanisms of dry and wet snow and the surface behave differently
Minimum numbers of required SAR images	2	2	1
SAR image requirements	Pair sensed at the same geometry	Pair has a short temporal baseline	Image has dual or quad polarizations
The complexity of the algorithms	Low	Medium	High
Primarily analyzed component	Backscattering coefficient	Coherence	Polarimetric parameters
LIA dependency	High	Medium	Low
The richness of derived information	Medium	Low	High
The noisiness of derived information	High	Low	Medium
Snow Type Sensing Capability			
Wet snow	Yes	No	Yes
Dry snow	No	No	Yes
Total snow	No	Yes	Yes

In addition to the aforementioned three main SAR-based approaches, other more elaborate possibilities should be further investigated, such as the information theoretic snow detection algorithm (ITSDA) proposed by Pettinato et al. [136]. A fusion of the three mainstream SAR-based approaches is another option: He et al. [163] facilitated the information derived from all three mainstream technique to a SVM classifier to map both dry and wet SCE; Tsai et al. [143] utilized RF to map total SCE based on backscatter, InSAR coherence, and PolSAR H/A/ α parameters in five study areas around the globe. The total and wet SCE estimated by Tsai et al. [143] is illustrated in Figure 11, which demonstrates the great value of fusing all three main SAR-based approaches to derive the holistic (total + wet) SCE. The holistic SCE enables not only investigating the dynamics of SCE and snowpack by comparing different seasons' SCE conditions but also the potential of further integration with conventional optical sensor-based cloud-affected SCE results.

When it comes to the ML classification method, considering the recent advances in deep learning (DL) algorithms and computer hardware, there have been few attempts utilizing the neural network to detect snow in SAR imagery, such as Usami et al. [180] and Nijhawan et al. [198], which showed a classification accuracy that was comparable to conventional ML algorithms.

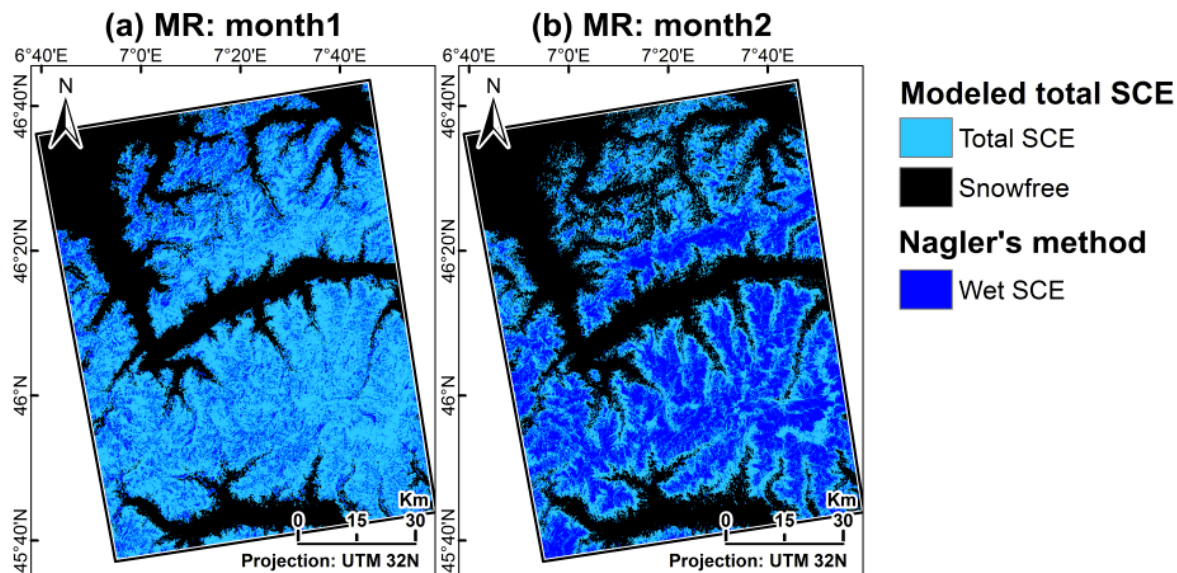


Figure 11. Total and wet SCE of Monte Rosa (MR) region (a) month1: 2018 March 12 (b) month2: 2018 May 11. Figures are revised from Tsai et al. [143]. Note the total SCE is modeled based on backscatter, InSAR coherence, and PolSAR parameters; wet SCE is estimated based on conventional backscatter-threshold approach.

5.3. Solutions for Addressing SAR-Vegetation Interaction

As mentioned in 4.2., the presence of vegetation would limit the viability of SAR-based snow cover classification approaches. The most successful algorithm specifically for forested regions was developed by Koskinen et al. [138], utilizing two reference images to minimize the effect of a forest. Based on that, Luojus et al. [139,175,189,199,200] accomplished several improvements resulting in the Helsinki University of Technology (TKK)-developed snow cover detection method aiming at boreal forest regions. Its forest compensation algorithm makes use of a semi-empirical forest backscattering model, which utilizes the stem volume information to estimate the amount of backscattering originating from the forest and further eliminates this factor from subsequent calculations.

However, in addition to the general problem of lower accuracy in open areas, the biggest limitation of the TKK method is that it requires prior knowledge of forest stem volumes, which is difficult to obtain. Thus, a purely spaceborne image-based approach to address the interaction between SAR imagery and vegetation needs to be developed. Hopefully, in the recent paper published by Tsai et al. [143], a land cover type-dependent classification strategy which can be applied to densely vegetated forest and agricultural regions was proposed. The method was tested in five mountainous study areas around the globe and the accuracy above 0.75 is confirmed in all regions by validation with optical-based SCE product. This study provides a novel way to map SCE in all land cover types and should be utilized in the future studies.

Additionally, the potential of utilizing PolSAR, Polarimetric Interferometric SAR (PolInSAR) as well as Tomographic SAR (TomoSAR) to estimate 3D forest structure and biomass [201–203] should be further integrated into current SAR-based snow cover detection algorithms to mitigate the negative effect of vegetation. This is also proposed in ESA's 7th Earth Explorer selected mission, BIOMASS (equipped with fully polarimetric P-band SAR, planned to launch in 2020) [204].

5.4. Influence of Filtering Algorithms

The speckle noise in SAR images affects all SAR-based snow cover detection algorithms, especially the backscattering-based approaches. The available options for filtering algorithms to overcome this problem include Frost filter [30,126,137,142,186,187,195], refined Lee filter [96,132,163,205,206],

median filter [102,103,131], low pass filter [135,207], multichannel intensity filter [140], binary partition tree [167], De Grandi filter [208], multi-scale multilooking [209], and Kuan filter [136]. Some studies attempted to compare the ability of different filters. Schellenberger et al. [134] used the effective number of looks (ENL) and standard deviations to compare the performance of median, Gamma DEMAP and Frost filter. Results showed that the median filter performs best in a purely statistical aspect; Frost filter, however, should be selected since the median filter is not an adaptive filter, which preserves image details while smoothing speckles by using unequal weights [210]. They also implied that the window size influences the performance of filters. Thakur et al. [102] preferred the median filter, as other filters might cause information loss at the pixel level. However, these studies only compared few filters and so far, no extensive comparison has been made to discuss the advantages and disadvantages of all available filters in a comprehensive overview.

5.5. Reliability of Current Validation Approaches

As shown in Figure 10, around half of the available studies employed snow cover classifications based on optical sensors as ground truth to validate the SAR-based snow cover results. This approach, however, can encounter several problems. First, for studies only aiming at wet snow monitoring, the date selection of optical images is critical. Usually, late spring is selected when the snowpack theoretically melts even in the highest elevation zones [140]. This would ensure that the SAR-based snow cover mapping detects the entire snow cover extent. However, it cannot be guaranteed that no dry snow is left.

Additionally, acquisition times of SAR and optical images differ. The resulting temporal gap leads to uncertainties, because melting processes, sudden snowfall or precipitation events all may result in different SCE in the optical and SAR data [175]. Most authors, however, selected the nearest sensed image pair, despite the time difference (e.g., 14 days between PALSAR and Landsat [169], 14 days between Radarsat-2 and Landsat [118], six days between PALSAR and AVNIR-2 [211]). Even though some satellites equipped with both SAR and optical sensors at the same platform (e.g., the Advanced Land Observation Satellite (ALOS)) may acquire both images at the same time, the presence of cloud may still hinder the optical observation.

Additionally, the difference between day and night might lead to great variations, as proven by studies investigating the top layer of a snowpack, which might refreeze after a cloud-free night with low temperatures. Such a refreeze event increases the surface backscattering significantly [67,186] and therefore would cause a high contrast between morning and evening observations [118]. Field surveys also revealed that the infiltration of rain may cause both, thick ice crusts within the snowpack as well as larger snow grains [184]. On top of that, differing magnitudes of temperature change in each elevation zone [65] impede the possibility to compensate its influence on the snowpack.

When validating SAR-based snow cover classifications with products derived from optical data, the accuracy of these reference datasets is of importance. Such products are often calculated applying a threshold of 0.4 NDSI, which might cause an underestimation as only pixels containing more than 50% of snow will be selected [212,213]. Some researchers therefore used 0.7 as a threshold to allow only fully snow covered pixels for detection [134,186]. In addition, limiting the optical-based snow cover detection to NDSI alone may introduce errors. It is generally advised to include additional tests, such as Landsat TM band4 ≥ 0.11 [214] and SPOT band3 ≥ 0.11 [215] or using an NDSI-NDVI threshold to address dense forest regions [216]. Even though the need for these additional tests is well-known in the optical snow cover community, SAR-based studies often fail to include these tests. Finally, as the spatial resolutions of SAR and optical images differ, the comparison procedures generally involve resampling operations [133], i.e., aggregating the higher resolution snow cover product to match the coarser one. Nevertheless, the definition of SCE in the coarser pixel may affect the validation significantly [140].

To overcome the constraints related to comparisons between optical and SAR-based snow cover classifications, a promising alternative approach is regional or global scale weather forecasting and/or snow models as suggested in Beniston et al. [23]. Although these models are criticized for their

comparatively low spatial resolution, dependency on empirical parameter setting [217,218] and the oversimplification of the snowpack [44], they can provide useful information such as ground temperature and snow accumulation amount [96,144]. As the complexity and spatial resolution of such models advance, they may constitute a notable alternative for future validation approaches of SAR-based snow cover products.

5.6. Opportunities of Data Fusion for SAR-Based Snow Cover Detection

5.6.1. SAR Flight Direction (Ascending and Descending)

In Nagler's study [140], merging ascending and descending SAR observations was mentioned as a crucial future development, which was also discussed in the Sentinel for science (SEN4SCI) scientific workshop [122]. It was also suggested that this combination could reduce the dependency of LIA [135,191]. However, only four studies utilized this solution, although Rott and Nagler already tested this approach in their pioneer paper [127]. In their paper, two ratio maps were masked with shadow and layover areas as well as regions containing extreme LIA. Then they combined the images pixel-wise based on the LIA value. Bartsch et al. [65] applied a similar approach but considered potential thawing. The general problem when combining different flight paths is the ground temperature difference between sensing times may lead to a change of the snowpack condition [67]. Thus, Bartsch et al. [65] recommended a separate classification threshold for each direction.

5.6.2. SAR Polarization (co- and Cross-Polarization)

Several studies indicated that the influence of LIA on the backscattering difference between dry and wet snow is also polarization-related, and that cross-polarization can preserve a better difference under small LIA conditions [140,219]. Hence, the combination of different polarizations could be a promising option. Nagler et al. [140] calculated the ratio map for VV and VH independently and fused them with their weights based on LIA. So far, however, no other study investigated this potential and, therefore, more research is required.

5.6.3. Combination of SAR with Optical Imagery

Although many studies referred to the benefit of synergizing cloud-penetrating SAR with the high spatial/temporal resolution of optical imagery, so far there are only very few studies available that actually followed this approach. In all reviewed studies, only 12 performed a fusion of optical- and SAR-based snow cover classifications. This implies that there is still some potential to develop a dedicated algorithm combining optical and SAR data for snow cover detection.

So far, most studies relied on optical-based NDSI calculation to map total SCE and then apply Nagler's method to map wet snow. Subsequently, dry, wet and total SCE can be derived [220–222]. This simple areal calculation, however, is not a genuine fusion of the same SCE type sensed by different sensors. A possible integration is to assign weights to both SAR-based and optical-based snow cover classifications as pursued by Malnes et al. [151], Solberg et al. [33] and Solberg et al. [68]. In these studies, time-series of SAR-based total SCE's were merged with total snow cover derived from MODIS by applying (1) confidence values assigned to each sensor's snow cover result, and (2) a time-dependent function defining how quickly the confidence value would decay over time. Ultimately, the algorithm would select the snow cover result with the highest confidence value for each pixel. Nevertheless, as those key parameters were selected by finding the optimal solution through trial and error, the case-dependency hinders transferability to other locations and periods. A more universally applicable combination procedure, however, is still lacking.

5.6.4. Combination of SAR with Passive Microwave Imagery

Theoretically, the temperature information sensed by passive microwave sensors would support analysis and detection of SCE, as the temperature of wet and dry snow and bare ground differs.

However, the coarse spatial resolution of passive microwave sensors aggravates an integration of this data into SAR processing. Moreover, Liu et al. [104] identified SAR-derived and passive microwave-derived SCE only match for 61%. They suggested this mismatch may be due to fact that the two sensors measure different temporal-physical snow parameters as the passive microwave sensor senses snow emissivity and brightness temperature, which can be analyzed for deriving snow depth and then linked to the actual SWE. In contrast, SAR records the backscattering representing long-term morphology processes prior to the sensing time. Consequently, combining the two data sources led to biased results, which represent different temporal-physical snow parameters. A similar magnitude of mismatch was also observed by Zhou and Zheng [96].

5.7. Overall Trajectory of Spaceborne SAR-Based SCE Detection and Future Possibilities

According to the available studies reviewed in the present paper, the overall trajectory of spaceborne SAR-based SCE detection may be summarized into three phases as depicted in Figure 12.

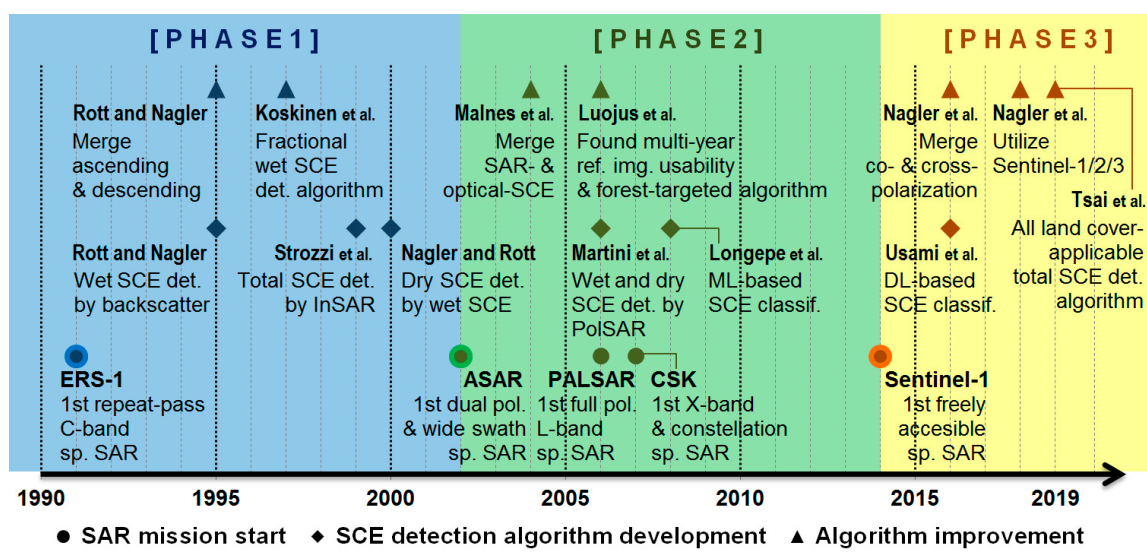


Figure 12. Overall development of algorithms and methods relying on spaceborne SAR data for snow cover extent (SCE) detection. The three phases denote the different main algorithms based on available SCE detection algorithms and SAR data.

After the launch of ERS-1 in 1991 and before the launch of ASAR in 2002, the repeat-pass imagery of ERS-1 allowed for a bi-temporal image analysis. Using this data source, Rott and Nagler developed their pioneer wet SCE mapping algorithm based on backscattering information [127]. The same applies to their dry SCE detection approach [126] as well as Strozzi et al.'s total SCE mapping with InSAR technique [147]. Moreover, merging different flight paths for achieving higher mapping accuracy [127] and calculating fractional SCE detection [138] were also proposed. In this phase, most of the available studies only utilized backscattering or InSAR techniques.

New breakthroughs were achieved in the second phase after the launch of ASAR and before the launch of Sentinel-1 in 2014. Dual/quadrupole-polarization, multi-band, and constellations of SAR sensors significantly stimulated the development of new snow cover detection methods. The rich information derived from PolSAR became achievable. For dealing with the overwhelming amount of parameters from this new source of information (Appendix A), machine learning classifications were introduced. In addition, various improvements of wet SCE mapping algorithms were achieved, including the combination with optical-based SCE [151], and proposing an algorithm with a multi-year usable reference image optimized for forest regions [139].

Topic has already shifted into the third phase since the launch of Sentinel-1 in 2014. In the hardware aspect, the fine spatial/temporal resolution and freely accessible Sentinel-1 offer an opportunity for long-term SAR-based SCE detection. Together with the prosperity of emerging X-band SAR sensors, more SAR-based studies are foreseeable such as integration and comparison of SCE information achieved from different bands of SAR sensors. In addition, the Sentinel series' satellites constellations significantly improve the potential of multi-sensor fusion as demonstrated in Nagler et al. [221]. In the algorithm aspect, thanks to the all land cover applicable total SCE detection approach proposed by Tsai et al. [143], it largely solves the previous studies' limitation that SAR-based approaches cannot detect snow accurately in vegetated regions and can only monitor wet SCE. This provides a great opportunity for future studies to integrate and complement SAR-based SCE with conventional optical-sensor-based cloud-affected SCE results to achieve more comprehensive SCE dynamics information in both spatial (conquering the influence of polar darkness and frequent cloud coverage, with ~20 m spatial resolution) and temporal (long time-series, daily temporal resolution) aspects. Another key development is DL, although only few studies exploited Sentinel-1 in combination with DL techniques so far, it is foreseeable that there will be further studies utilizing it to solve the current technical challenges, including the influence of different filtering algorithms, impact of different sensing geometry, less classification accuracy in the forest regions, and fusion of heterogeneous sensors' such as Light detection and ranging (Lidar) as well as passive sensors. In validation aspect; the need of proper validation for SAR-based SCE—especially wet SCE—still needs to be addressed. Most of the previous studies did not provide reliable validation due to the limitation of sparse in situ measurements. Finally, in the application aspect, as previous studies did not fully utilize the benefit that SAR can distinguish wet and dry SCE, but only regard the wet SCE as total SCE during snow melting season [140], the information of wet SCE which cannot be derived from conventional optical-based approach (can only detect total SCE) should be further utilized.

Consequently, based on the trajectory and the recent developments of SAR sensors and snow detection algorithms, it can be expected that in the near future once the SAR-based SCE detection approach (1) achieves daily temporal resolution by fusing different SAR sensors' information (2) reaches satisfactory classification accuracy and global transferability as proved by Tsai et al. [143]; SAR-based monitoring approach would replace the conventional optical-sensor-based SCE detection approach as more snowpack information can be inferred (such as wet or dry and surface roughness) and can fundamentally solve the cloud coverage and polar darkness issues.

5.8. Difficulties of Sensing Additional Snow Parameters

SWE and SD are two commonly desired snow parameters as both of them can be used to estimate the amount of water stored within a snowpack. So far, there are numerous studies aiming to identify the relationship between the information stored in SAR data and SWE as well as SD. At present, however, there is no solid conclusion to solve this challenge since various other factors affect the interactions between SAR signals and both, SWE and SD. The wetness of the snowpack, for example, would change the relative surface roughness and further affect SAR backscatter [106]. The correlation between backscattering and SWE would therefore vary with the conditions of snow, soil [223], and the surface roughness [92]. The relationship between SD and SAR also links to grain size, snow density, melting conditions, and temperature [188,220]. Simulations suggest that the backscattering would increase with SD in a coarse-grained snowpack, but decrease in a fine-grained snowpack [96]. Consequently, it is unreliable to derive SWE or SD merely from SAR information as it either requires inversions or empirical models [98,152,224,225].

6. Conclusions

Snow cover extent is one of the most important cryospheric components, as it controls global radiation balance, hydrological behavior, vegetation coverage and affects human activities. Spaceborne SAR offers the capability to quantify snow cover conditions even under clouded or

nighttime conditions, which enables a better understanding of the global snow cover dynamics. Moreover, its polarizations and phase data provide valuable information about the snowpack characteristics. Three mainstream SAR-based approaches to map snow cover have been pursued in last three decades: (1) Detecting wet snow based on SAR backscattering behavior; (2) PolSAR technique inverting the scattering mechanism of the targeted snow type; and (3) the coherence value calculated from InSAR techniques enabling estimation of total SCE.

After evaluating relevant studies published within the last three decades, we draw the following conclusions for monitoring snow cover using spaceborne SAR:

- (1) C-band SAR based algorithms dominate the studies, but the recent prosperity of X-band SAR provides a promising option. Due to the long-term preference of the C-band wavelength and its better capability to detect snow when compared to L-band SAR, C-band SAR has the longest history and is utilized for snow cover detection more often than any other sensor. However, many recent studies have proven that X-band is more suitable to detect dry snow; considering the amount of new and planned X-band missions, an increase in popularity of X-band based snow cover detection algorithms therefore can be expected for the near future.
- (2) Most studies focused on mountainous regions, especially the European Alps (32%) and the Asian Himalaya (31%), leading to an imbalanced distribution of study sites. The relatively small size of the study sites also implies the lack of utility of the recent wide-swath sensing mode.
- (3) The majority of studies investigated snow cover for one year with an average of two observations within this year to account for the dynamics of the snowpack. These temporal aspect-limited studies indicate that there is still a gap in understanding the long-term capability of SAR-based algorithms to detect snow consistently.
- (4) For detecting wet SCE, the majority of studies relied on backscattering-based approaches. More than 55% of the reviewed studies only detected wet snow, with 82% of those studies applying a backscattering-based approach proposed by Nagler et al. in 2000. However, we observed a recent increase in studies relying on InSAR- and PolSAR-based algorithms especially for the detection of dry and total SCE.
- (5) This review confirms the importance of ancillary data such as a DEM, a land cover map as well as meteorological data as additional inputs into SAR-based snow detection algorithms. Based on the DEM data, information about LIA, SAR shadow and layover can be derived; land cover information is useful to mitigate the negative effects of vegetated areas on the classification accuracy, and the actual snow melting conditions can be inferred from meteorological data.
- (6) Commonly employed classification methods shifted from supervised ML approach towards more sophisticated DL approaches, and the maturity of optical-based snow cover products enables a selection of suitable training samples for supervised classifications.
- (7) Technical advances in recently launched SAR missions such as wider sensing swaths, shorter revisit times and quad-polarization make SAR-based snow cover detection more promising. These technical developments and the mainstream SAR-based algorithms complement each other well, as the extended coverage can increase the efficiency of the classification, the shortened revisiting time can support InSAR-based approaches to sustain more usable coherence, and the quad-polarization can enrich the information decomposed by PolSAR-based techniques.
- (8) The difficulty of SCE detection in vegetated land cover regions is recently addressed but further exploration of PolInSAR and TomoSAR techniques should be investigated. In addition, the influence of filter algorithms on the quality of the final snow cover product requires additional research.
- (9) The synergy of SAR with other sensors (e.g., optical and passive microwave) to improve the quality of snow cover classifications is still immature and requires further research. The synergic use with other sensors may also help develop and establish generally accepted validation strategies.

- (10) Thanks to the characteristics of SAR which can penetrate through clouds and sense ground independently of solar illumination conditions, together with the recent prosperity of different SAR satellites and advancement of ML/DL algorithms, it is foreseeable that SAR-based SCE detection approaches can complement conventional optical sensor-based SCE detection approaches in the near future as SAR provides more snowpack condition information and can fundamentally solve the cloud coverage and polar darkness limitations.

Author Contributions: Conceptualization, Y.S.T., A.D. and C.K.; Writing, Y.S.T.; Review and Editing, A.D., C.K., and N.O.; Supervision, A.D., C.K., and N.O.

Funding: This research received no external funding.

Acknowledgments: Support by the German Academic Exchange Service (DAAD) fellowship to Ya-Lun S. Tsai is gratefully acknowledged.

Conflicts of Interest: The authors declare no conflict of interest.

Appendix A

Table A1. The summary of included studies' SCE monitoring strategy (targeted snow type, classification method and data synergy).

Band	Sensor	Wet Snow		Dry Snow		Total Snow		Classification	Synergy		
		Employed Approach				Supervised	Un-Supervised				
		Backscatter	PolSAR	InSAR	Topo-Based						
X-Band	COSMO-SkyMed	[134,136,137, 186–188,220, 226]			[134]						
	TerraSAR-X	[86,136,184, 227,228]	[209]	[148,194,229]	[227]	[194,228,229]			[194,228,229]		
C-Band	ERS-1/2	[85,121,126, 127,135,138, 139,155,156, 206,207,230, 231]		[185,232]	[126]				[126]		
	Radatsat-1	[103,104,121, 126,131,133, 141,175,176, 189,199,200, 206,233–236]			[131]						
L-Band	ENVISAT	[33,65,68, 102,132,142, 145,151,153– 156,195,206, 237–245]		[145,185]	[33,68,151, 153–156,237, 238,240,241, 243–245]			[185]	[65,142]		
	Radarsat-2	[35,152,163, 177,184,205, 246]	[35,159,163, 165,177,209]	[163]	[152]	[35,163,167, 205,246]	[118,149,168, 191,208]	[149,163,165, 177,191,208, 246]	[168]		
	Sentinel-1	[96,140,143, 221,222,247– 249]			[96]		[143,198,250]	[143,198]	[221,222]		
	ALOS-1		[169,174,251]			[174]	[30,144,170, 171,211,251, 252]	[30,174]	[211,252]		
	ALOS-2		[180]				[180]				

Table A2. Summary of included studies' SCE monitoring strategy (studying region type, validation data and usage of land cover information).

Band	Study Regions Type				Validation Dataset			Land Cover	
	Mountainous	Forest	Glacier	Landsat	MODIS	AVNIR-2	Aerial	Involved Analysis	Only Mask
X-Band	COSMO-SkyMed	[134,136,137, 186–188,220, 226]			[134,136,137, 186,187,226]				[136,186,226]
	TerraSAR-X	[86,136,209, 227]	[148]	[194,228,229]					
ERS-1/2	[85,126,135, 231,232]	[138,139,230]		[126,232]				[121]	[121,139,230]
Radatsat-1	[103,131,133, 176,233,234]	[175,189,199, 200,235,236]	[104]		[175,189,199, 200,235,236]		[103,133]	[175,189,199, 200,235,236]	
C-Band	ENVISAT	[33,65,68, 102,132,151, 153–156,195, 237–245]		[142,145,185, 206]	[68]	[102,151,153, 154,237]		[68]	[238,241,244]
	Radarsat-2	[35,118,149, 152,159,163, 167,168,205, 208,246]	[168]	[165,177,191]	[35,118,159, 163,168,191, 205]	[152]			[118,149,163, 165]
Sentinel-1	[140,143,198, 221,222,247– 250]	[143]	[96]	[140,143]	[143]			[143]	[143]
L-Band	ALOS-1	[30,144,169, 171,211,252]		[251]	[169]		[30,169,170, 211]		
	ALOS-2	[180]							

Table A3. The PolSAR decomposition techniques and parameters employed in the included studies.

Decomposition Type	Parameter	Wet and Dry Snow Response	Total Snow Response	Employed by Studies	Used for Final Classification	
					Wet and Dry Snow	Snow-Covered/Free
Backscattering	B_{HH}, B_{HV} B_{VH}, B_{VV}			[165,174]	B_{HV} [165]	B_{HV} [169]
Pauli decomposition [160]	Cloude and Pottier 1996	P_{odd} single/odd bounce, P_{dbl} double/even bounce, P_{vol} volume scattering	Low P_{dbl} and P_{vol} [169]	[30,35,163,165,167–169]	P_{vol} [163] P_{dbl} [165] All [174]	All [174]
H/A/ $\bar{\alpha}$ [160]	Cloude and Pottier 1996	H entropy A anisotropy $\bar{\alpha}$ angle $\lambda_1, \lambda_2, \lambda_3$ 1-H H(1-A)	Low λ_3 for wet snow [30] Low $\bar{\alpha}$ for wet snow [35] High H for wet snow [35]	Low H and H(1-A) [30] Low H, $\bar{\alpha}$ [251] High A [30]	[30,35,118,143,163,165,167,169,171,172,174,191,211,246,251,252] λ_3 [163,246] H/ $\bar{\alpha}$ [35]	λ_3 [30,171] $\lambda_1, \lambda_2, \lambda_3, \bar{\alpha}$ [191] H [168,169,211] A [168,211] $\bar{\alpha}$ [211]
Freeman [253]	Freeman and Durden 1998	F_{odd} surface, F_{dbl} double-bounce, F_{vol} volume scattering		[163,169,174,211]		
Yamaguchi [254]	Yamaguchi et al. 2006	Helix scattering of Y_{hlx} coefficient, Y_{odd} surface, Y_{dbl} double-bounce, Y_{vol} volume scattering P_s, P_d, P_v, P_c		[30,163,169,211,246]	Y_v [163,246]	
Touzi [255]	Touzi 2007	ψ_1, ψ_2, ψ_3 $\tau_1, \tau_2, \psi\tau_3$ $\alpha_1, \alpha_2, \alpha_3$ ϕ_1, ϕ_2, ϕ_3		[168]		ψ_1 [191] τ_1, τ_2 [168]
[256]	Antropov et al. 2011	Generalized volume scattering		[159]		
Kennaugh [257]	Schmitt et al. 2015	Kennaugh elements $K_1 \sim K_9$	Low K_0 for wet snow [209]	[209]	K_0 [209]	

Table A3. Cont.

Decomposition Type	Parameter	Wet and Dry Snow Response	Total Snow Response	Employed by Studies	Used for Final Classification	
					Wet and Dry Snow	Snow-Covered/Free
Derived parameter						
	Total power (TP)		Low TP [251]	[251]		
Van Zyl et al. 1987	Polarization fraction (PF) [258]	High PF for wet snow [118]	High PF [251]	[30,118,171,251]		[30,118,171]
Ainsworth et al. 2002	Polarimetric asymmetry (PA) [259]		High PA [30]	[30]		
Lüneburg 2001	Lüneburg anisotropy (LA) [260]		Low LA [30]	[30]		
Allain et al. 2006	single-bounce eigenvalue relative difference (SERD) double-bounce eigenvalue relative difference (DERD) [261]	High SERD when snow is wet as the surface scattering dominates [35]		[30,35]	SERD [35]	
Lee and Pottier 2009	Copolarization Coherence [262]		[30]			
Lee and Pottier 2009	polarimetric copolarization phase difference (PPD) [262]		[30]			
	Huynen parameter A_0		[174]			
	Radar Vegetation Index (RVI)		[174]			
	Degree of polarization (DoP)		[180]			

References

1. Pepe, M.P.L.; Brivio, P.A.; Rampini, A.; Nodari, F.R.; Boschetti, M. Snow cover monitoring in Alpine regions using ENVISAT optical data. *Int. J. Remote Sens.* **2005**, *26*, 4661–4667. [[CrossRef](#)]
2. Lemke, P.; Ren, J.; Alley, R.B.; Allison, I.; Carrasco, J.; Flato, G.; Fujii, Y.; Kaser, G.; Mote, P.; Thomas, R.H.; et al. *Observations: Changes in Snow, Ice and Frozen Ground*; Cambridge University Press: Cambridge, UK, 2007.
3. Kerr, Y.; Mahmoodi, A.; Mialon, A.; Al Biltar, A.; Rodríguez-Fernández, N.; Richaume, P.; Cabot, F.; Wigneron, J.; Waldteufel, P.; Ferrazzoli, P.; et al. *Soil Moisture Retrieval Algorithms: The SMOS Case*; Elsevier: Amsterdam, The Netherlands, 2018; pp. 156–190.
4. GCOS, WMO. *Systematic Observation Requirements for Satellite-Based Data Products for Climate—2011 Update*; GCOS, WMO: Geneva, Switzerland, 2011.
5. Metsämäki, S.; Ripper, E.; Mattila, O.-P.; Fernandes, R.; Schwaizer, G.; Luojus, K.; Nagler, T.; Bojkov, B.; Kern, M. Evaluation of Northern Hemisphere and regional snow extent products within ESA SnowPEx-project. In Proceedings of the 2017 IEEE International Geoscience and Remote Sensing Symposium (IGARSS), Fort Worth, TX, USA, 23–28 July 2017.
6. Dietz, A.J.; Kuenzer, C.; Dech, S. Global SnowPack: A new set of snow cover parameters for studying status and dynamics of the planetary snow cover extent. *Remote Sens. Lett.* **2015**, *6*, 844–853. [[CrossRef](#)]
7. Kim, E.; Gatebe, C.; Hall, D.; Newlin, J.; Misakonis, A.; Elder, K.; Marshall, H.P.; Heimstra, C.; Brucker, L.; De Marco, E. Overview of SnowEx Year 1 Activities. In Proceedings of the SnowEx Workshop 2017, Longmont, CO, USA, 8–10 August 2017.
8. Manuel, G.; Gascoin, S.; Hagolle, O.; L'helguen, C.; Klempka, T. Let it snow—Operational snow cover product from Sentinel-2 and Landsat-8 data. In Proceedings of the Living Planet Symposium 2016, Prague, Czech Republic, 9–13 May 2016.
9. Trofaier, A.M. Monitoring Snow & Ice from space. In Proceedings of the Copernicus Pan European High Resolution Snow and Ice Monitoring Product-User Consultation Workshop, Etterbeek, Belgium, 7 June 2018.
10. Barry, R.G. The parameterization of surface albedo for sea ice and its snow cover. *Prog. Phys. Geogr. Earth Environ.* **1996**, *20*, 63–79. [[CrossRef](#)]
11. Barry, R.G.; Chorley, R.J. *Atmosphere, Weather and Climate*; Routledge: London, UK, 2009.
12. Serreze, M.C.; Walsh, J.E.; Chapin, F.S., III; Osterkamp, T.; Dyurgerov, M.; Romanovsky, V.; Oechel, W.C.; Morison, J.; Zhang, T.; Barry, R.G. Observational Evidence of Recent Change in the Northern High-Latitude Environment. *Clim. Chang.* **2000**, *46*, 159–207. [[CrossRef](#)]
13. Barnett, T.P.; Adam, J.C.; Lettenmaier, D.P. Potential impacts of a warming climate on water availability in snow-dominated regions. *Nature* **2005**, *438*, 303–309. [[CrossRef](#)] [[PubMed](#)]
14. Scherrer, S.C.; Ceppi, P.; Croci-Maspoli, M.; Appenzeller, C. Snow-albedo feedback and Swiss spring temperature trends. *Theor. Appl. Clim.* **2012**, *110*, 509–516. [[CrossRef](#)]
15. Kevin, J.-P.W.; Kotlarski, S.; Scherrer, S.C.; Schär, C. The Alpine snow-albedo feedback in regional climate models. *Clim. Dyn.* **2017**, *48*, 1109–1124.
16. Armstrong, R.L.; Brodzik, M.J. Hemispheric-scale comparison and evaluation of passive-microwave snow algorithms. *Ann. Glaciol.* **2002**, *34*, 38–44. [[CrossRef](#)]
17. Dankers, R.; De Jong, S.M. Monitoring snow-cover dynamics in Northern Fennoscandia with SPOT VEGETATION images. *Int. J. Remote Sens.* **2004**, *25*, 2933–2949. [[CrossRef](#)]
18. Steffen, K. Surface energy exchange at the equilibrium line on the Greenland ice sheet during onset of melt. *Ann. Glaciol.* **1995**, *21*, 13–18. [[CrossRef](#)]
19. Vaughan, D.G.; Comiso, J.C.; Allison, I.; Carrasco, J.; Kaser, G.; Kwok, R.; Mote, P.; Murray, T.; Paul, F.; Ren, J.; et al. Observations: Cryosphere. *Clim. Chang.* **2013**, *2103*, 317–382.
20. Yang, Y.; Leppäranta, M.; Cheng, B.; Li, Z. Numerical modelling of snow and ice thicknesses in Lake Vanajavesi, Finland. *Tellus A* **2012**, *64*, 17202. [[CrossRef](#)]
21. Ebert, E.E.; Curry, J.A. An intermediate one-dimensional thermodynamic sea ice model for investigating ice-atmosphere interactions. *J. Geophys. Res. Space Phys.* **1993**, *98*, 10085–10109. [[CrossRef](#)]
22. Shine, K.P.; Henderson-Sellers, A.; Henderson-Sellers, A. The sensitivity of a thermodynamic sea ice model to changes in surface albedo parameterization. *J. Geophys. Res. Space Phys.* **1985**, *90*, 2243–2250. [[CrossRef](#)]

23. Beniston, M.; Farinotti, D.; Stoffel, M.; Andreassen, L.M.; Coppola, E.; Eckert, N.; Fantini, A.; Giacona, F.; Hauck, C.; Huss, M.; et al. The European mountain cryosphere: A review of its current state, trends, and future challenges. *Cryosphere* **2018**, *12*, 759–794. [[CrossRef](#)]
24. Déry, S.J.; Romanovsky, V.E.; Stieglitz, M.; Osterkamp, T.E. The role of snow cover in the warming of arctic permafrost. *Geophys. Res. Lett.* **2003**, *30*, 13.
25. Pogliotti, P.; Guglielmin, M.; Cremonese, E.; Di Cella, U.M.; Filippa, G.; Pellet, C.; Hauck, C. Warming permafrost and active layer variability at Cime Bianche, Western European Alps. *Cryosphere* **2015**, *9*, 647–661. [[CrossRef](#)]
26. Zhao, J.-Y.; Chen, J.; Wu, Q.-B.; Hou, X. Snow cover influences the thermal regime of active layer in Urumqi River Source, Tianshan Mountains, China. *J. Mt. Sci.* **2018**, *15*, 2622–2636. [[CrossRef](#)]
27. Magnin, F.; Westermann, S.; Pogliotti, P.; Ravanel, L.; Deline, P.; Malet, E. Snow control on active layer thickness in steep alpine rock walls (Aiguille du Midi, 3842 m asl, Mont Blanc massif). *Catena* **2017**, *149*, 648–662. [[CrossRef](#)]
28. Beniston, M.; Stoffel, M.; Hill, M. Impacts of climatic change on water and natural hazards in the Alps: Can current water governance cope with future challenges? Examples from the European “ACQWA” project. *Environ. Sci. Policy* **2011**, *14*, 734–743. [[CrossRef](#)]
29. Huss, M.; Bookhagen, B.; Huggel, C.; Jacobsen, D.; Bradley, R.; Clague, J.; Vuille, M.; Buytaert, W.; Cayan, D.; Greenwood, G.; et al. Toward mountains without permanent snow and ice. *Earth’s Future* **2017**, *5*, 418–435. [[CrossRef](#)]
30. Singh, G.; Venkataraman, G.; Yamaguchi, Y.; Park, S.-E. Capability Assessment of Fully Polarimetric ALOS-PALSAR Data for Discriminating Wet Snow from Other Scattering Types in Mountainous Regions. *IEEE Trans. Geosci. Remote Sens.* **2014**, *52*, 1177–1196. [[CrossRef](#)]
31. Barnett, T.P.; Dümenil, L.; Schlese, U.; Roeckner, E.; Latif, M. The Effect of Eurasian Snow Cover on Regional and Global Climate Variations. *J. Atmos. Sci.* **1989**, *46*, 661–686. [[CrossRef](#)]
32. Schober, J.; Schneider, K.; Helffricht, K.; Schattan, P.; Achleitner, S.; Schöberl, F.; Kirnbauer, R. Snow cover characteristics in a glacierized catchment in the Tyrolean Alps—Improved spatially distributed modelling by usage of Lidar data. *J. Hydrol.* **2014**, *519*, 3492–3510. [[CrossRef](#)]
33. Solberg, R.; Amlien, J.; Koren, H.; Eikvil, L.; Malnes, E.; Storvold, R. Multi-sensor/multitemporal approaches for snow cover area monitoring. In Proceedings of the EARSeL LIS-SIG Workshop, Berne, Switzerland, 21–23 February 2005.
34. Serreze, M.C.; Clark, M.P.; Frei, A. Characteristics of large snowfall events in the montane western United States as examined using snowpack telemetry (SNOWTELE) data. *Water Resour. Res.* **2001**, *37*, 675–688. [[CrossRef](#)]
35. Dedieu, J.; De Farias, G.B.; Castaings, T.; Allain-Bailhache, S.; Pottier, É.; Durand, Y.; Bernier, M. Interpretation of a RADARSAT-2 fully polarimetric time-series for snow cover studies in an Alpine context—First results. *Can. J. Remote Sens.* **2012**, *38*, 336–351. [[CrossRef](#)]
36. Weingärtner, R.; Barben, M.; Spreafico, M. Floods in mountain areas—An overview based on examples from Switzerland. *J. Hydrol.* **2003**, *282*, 10–24. [[CrossRef](#)]
37. Romanov, P.; Gutman, G.; Csizsar, I. Automated Monitoring of Snow Cover over North America with Multispectral Satellite Data. *J. Appl. Meteorol.* **2000**, *39*, 1866–1880. [[CrossRef](#)]
38. Kvambekk, Å.S.; Melvold, K. Long-term trends in water temperature and ice cover in the subalpine lake, Øvre Heimdalsvatn, and nearby lakes and rivers. *Hydrobiologia* **2010**, *642*, 47–60. [[CrossRef](#)]
39. Favier, P.; Bertrand, D.; Eckert, N.; Naaim, M. A reliability assessment of physical vulnerability of reinforced concrete walls loaded by snow avalanches. *Nat. Hazards Earth Syst. Sci.* **2014**, *14*, 689–704. [[CrossRef](#)]
40. Mock, C.J.; Birkeland, K.W. Snow Avalanche Climatology of the Western United States Mountain Ranges. *Bull. Am. Meteorol. Soc.* **2000**, *81*, 2367–2392. [[CrossRef](#)]
41. Ancey, C.; Bain, V. Dynamics of glide avalanches and snow gliding. *Rev. Geophys.* **2015**, *53*, 745–784. [[CrossRef](#)]
42. Pielke, R.A.; Doesken, N.; Bliss, O.; Green, T.; Chaffin, C.; Salas, J.D.; Woodhouse, C.A.; Lukas, J.J.; Wolter, K. Drought 2002 in Colorado: An Unprecedented Drought or a Routine Drought? *Pure Appl. Geophys.* **2005**, *162*, 1455–1479. [[CrossRef](#)]
43. Schmucki, E.; Marty, C.; Fierz, C.; Weingartner, R.; Lehning, M. Impact of climate change in Switzerland on socioeconomic snow indices. *Theor. Appl. Climatol.* **2017**, *127*, 875–889. [[CrossRef](#)]

44. Steiger, R.; Abegg, B. The Sensitivity of Austrian Ski Areas to Climate Change. *Tour. Plan. Dev.* **2013**, *10*, 480–493. [[CrossRef](#)]
45. Jylhä, K.; Fronzek, S.; Tuomenvirta, H.; Carter, T.R.; Ruosteenoja, K. Changes in frost, snow and Baltic sea ice by the end of the twenty-first century based on climate model projections for Europe. *Clim. Chang.* **2008**, *86*, 441–462. [[CrossRef](#)]
46. Brown, R.D.; Robinson, D.A. Northern Hemisphere spring snow cover variability and change over 1922–2010 including an assessment of uncertainty. *Cryosphere* **2011**, *5*, 219–229. [[CrossRef](#)]
47. McCabe, G.J.; Wolock, D.M. Long-term variability in Northern Hemisphere snow cover and associations with warmer winters. *Clim. Chang.* **2010**, *99*, 141–153. [[CrossRef](#)]
48. Brown, R.; Derksen, C.; Wang, L. A multi-data set analysis of variability and change in Arctic spring snow cover extent, 1967–2008. *J. Geophys. Res. Space Phys.* **2010**, *115*, 16. [[CrossRef](#)]
49. Dye, D.G. Variability and trends in the annual snow-cover cycle in Northern Hemisphere land areas, 1972–2000. *Hydrol. Process.* **2002**, *16*, 3065–3077. [[CrossRef](#)]
50. Najafi, M.R.; Zwiers, F.W.; Gillett, N.P. Attribution of the spring snow cover extent decline in the Northern Hemisphere, Eurasia and North America to anthropogenic influence. *Clim. Chang.* **2016**, *136*, 571–586. [[CrossRef](#)]
51. Hori, M.; Sugiura, K.; Kobayashi, K.; Aoki, T.; Tanikawa, T.; Kuchiki, K.; Niwano, M.; Enomoto, H. A 38-year (1978–2015) Northern Hemisphere daily snow cover extent product derived using consistent objective criteria from satellite-borne optical sensors. *Remote Sens. Environ.* **2017**, *191*, 402–418. [[CrossRef](#)]
52. Pachauri, R.K.; Allen, M.R.; Barros, V.R.; Broome, J.; Cramer, W.; Christ, R.; Church, J.A.; Clarke, L.; Dahe, Q.; Dasgupta, P.; et al. *Climate Change 2014: Synthesis Report. Contribution of Working Groups I, II and III to the Fifth Assessment Report of the Intergovernmental Panel on Climate Change*; IPCC: Geneva, Switzerland, 2014.
53. Marty, C.; Schlägl, S.; Bavay, M.; Lehning, M. How much can we save? Impact of different emission scenarios on future snow cover in the Alps. *Cryosphere* **2017**, *11*, 517–529. [[CrossRef](#)]
54. Dietz, A.J.; Conrad, C.; Kuenzer, C.; Gesell, G.; Dech, S. Identifying Changing Snow Cover Characteristics in Central Asia between 1986 and 2014 from Remote Sensing Data. *Remote Sens.* **2014**, *6*, 12752–12775. [[CrossRef](#)]
55. Bulygina, O.N.; Groisman, P.Y.; Razuvaev, V.N.; Korshunova, N.N. Changes in snow cover characteristics over Northern Eurasia since 1966. *Environ. Res. Lett.* **2011**, *6*, 045204. [[CrossRef](#)]
56. Terzaghi, S.; Fratianni, S.; Cremonini, R. Winter precipitation in Western Italian Alps (1926–2010). *Meteorol. Atmos. Phys.* **2013**, *119*, 125–136. [[CrossRef](#)]
57. Dyrrdal, A.V.; Saloranta, T.; Skaugen, T.; Strandén, H.B. Changes in snow depth in Norway during the period 1961–2010. *Hydrol. Res.* **2013**, *44*, 169–179. [[CrossRef](#)]
58. Schmucki, E.; Marty, C.; Fierz, C.; Lehning, M. Simulations of 21st century snow response to climate change in Switzerland from a set of RCMs. *Int. J. Climatol.* **2015**, *35*, 3262–3273. [[CrossRef](#)]
59. Magnusson, J.; Jonas, T.; López-Moreno, I.; Lehning, M. Snow cover response to climate change in a high alpine and half-glacierized basin in Switzerland. *Hydrol. Res.* **2010**, *41*, 230–240. [[CrossRef](#)]
60. Dietz, A.J.; Kuenzer, C.; Gessner, U.; Dech, S. Remote sensing of snow—A review of available methods. *Int. J. Remote Sens.* **2012**, *33*, 4094–4134. [[CrossRef](#)]
61. König, M.; Winther, J.-G.; Isaksson, E. Measuring snow and glacier ice properties from satellite. *Rev. Geophys.* **2001**, *39*, 1–27. [[CrossRef](#)]
62. Bruder, J.A. IEEE Radar standards and the radar systems panel. *IEEE Aerosp. Electron. Syst. Mag.* **2013**, *28*, 19–22. [[CrossRef](#)]
63. Wiley, C.A. Synthetic aperture radars. *IEEE Trans. Aerosp. Electron. Syst.* **1985**, *3*, 440–443. [[CrossRef](#)]
64. Chan, Y.K.; Koo, V.C. An introduction to synthetic aperture radar (SAR). *Prog. Electromagn. Res. B* **2008**, *2*, 27–60. [[CrossRef](#)]
65. Bartsch, A.; Jansa, J.; Schöner, M.; Wagner, W. Monitoring of spring snowmelt with Envisat ASAR WS in the Eastern Alps by combination of ascending and descending orbits. In Proceedings of the Envisat Symposium, Montreux, Switzerland, 23–27 April 2007.
66. Campbell, B.A. *Radar Remote Sensing of Planetary Surfaces*; Cambridge University Press: Cambridge, UK, 2002.
67. Floricioiu, D.; Rott, H. Seasonal and short-term variability of multifrequency, polarimetric radar backscatter of Alpine terrain from SIR-C/X-SAR and AIRSAR data. *IEEE Trans. Geosci. Remote Sens.* **2001**, *39*, 2634–2648. [[CrossRef](#)]

68. Solberg, R.; Koren, H.; Amlien, J.; Malnes, E.; Schuler, D.V.; Orthe, N.K. The development of new algorithms for remote sensing of snow conditions based on data from the catchment of Øvre Heimdalsvatn and the vicinity. *Hydrobiologia* **2010**, *642*, 35–46. [[CrossRef](#)]
69. Macander, M.J.; Swingley, C.S.; Joly, K.; Raynolds, M.K. Landsat-based snow persistence map for northwest Alaska. *Remote Sens. Environ.* **2015**, *163*, 23–31. [[CrossRef](#)]
70. Harrison, A.R.; Lucas, R.M. Multi-spectral classification of snow using NOAA AVHRR imagery. *Int. J. Remote Sens.* **1989**, *10*, 907–916. [[CrossRef](#)]
71. Goldstein, R.M.; Engelhardt, H.; Kamb, B.; Frolich, R.M. Satellite Radar Interferometry for Monitoring Ice Sheet Motion: Application to an Antarctic Ice Stream. *Science* **1993**, *262*, 1525–1530. [[CrossRef](#)]
72. Zebker, H.A.; Goldstein, R.M. Topographic mapping from interferometric synthetic aperture radar observations. *J. Geophys. Res. Space Phys.* **1986**, *91*, 4993–4999. [[CrossRef](#)]
73. Touzi, R.; Lopes, A.; Bruniquel, J.; Vachon, P. Coherence estimation for SAR imagery. *IEEE Trans. Geosci. Remote Sens.* **1999**, *37*, 135–149. [[CrossRef](#)]
74. Kim, J.-R.; Lin, S.-Y.; Yun, H.-W.; Tsai, Y.-L.; Seo, H.-J.; Hong, S.; Choi, Y. Investigation of Potential Volcanic Risk from Mt. Baekdu by DInSAR Time Series Analysis and Atmospheric Correction. *Remote Sens.* **2017**, *9*, 138. [[CrossRef](#)]
75. Tsai, Y.; Lin, S.; Kim, J. Tracking Greenland Russell Glacier Movements Using Pixel-offset Method. *J. Photogramm. Remote Sens.* **2018**, *23*, 173–189.
76. Tsai, Y.-L.; Kim, J.-R.; Save, H.; Lin, S.-Y. Monitoring Groundwater Depletion of Northwest India using SAR Interferometry. In *AGU Fall Meeting Abstracts*; American Geophysical Union: Washington, DC, USA, 2016.
77. Taini, G.; Pietropaolo, A.; Notarantonio, A. Criteria and trade-offs for LEO orbit design. In Proceedings of the 2008 IEEE Aerospace Conference, Big Sky, MT, USA, 1–8 March 2008.
78. Luo, X.; Wang, M.; Dai, G.; Chen, X. A Novel Technique to Compute the Revisit Time of Satellites and Its Application in Remote Sensing Satellite Optimization Design. *Int. J. Aerosp. Eng.* **2017**, *2017*, 6469439. [[CrossRef](#)]
79. Dial, G.; Bowen, H.; Gerlach, F.; Grodecki, J.; Oleszczuk, R. IKONOS satellite, imagery, and products. *Remote Sens. Environ.* **2003**, *88*, 23–36. [[CrossRef](#)]
80. Key, J.; Drinkwater, M.; Ukita, J. IGOS cryosphere theme report. *WMO/TD* **2007**, *1405*, 100.
81. Curlander, J.C.; McDonough, R.N. *Synthetic Aperture Radar*; John Wiley & Sons: New York, NY, USA, 1991.
82. Lillesand, T.M.; Kiefer, R.W. *Remote Sensing and Photo Interpretation*; John Wiley and Sons: New York, NY, USA, 1994; p. 750.
83. Chan, A.K.; Peng, C. *Wavelets for Sensing Technologies*; Artech House: Norwood, MA, USA, 2003.
84. Ulaby, F.T.; Stiles, W.H. The active and passive microwave response to snow parameters: Water equivalent of dry snow. *J. Geophys. Res. Space Phys.* **1980**, *85*, 1045–1049. [[CrossRef](#)]
85. Salcedo, A.P.; Cogliati, M.G. Snow Cover Area Estimation Using Radar and Optical Satellite Information. *Atmos. Clim. Sci.* **2014**, *4*, 514–523. [[CrossRef](#)]
86. Besic, N.; Vasile, G.; Dedieu, J.-P.; Chanussot, J.; Stanković, S. Stochastic Approach in Wet Snow Detection Using Multitemporal SAR Data. *IEEE Geosci. Remote Sens. Lett.* **2015**, *12*, 244–248. [[CrossRef](#)]
87. Mätzler, C. Applications of the interaction of microwaves with the natural snow cover. *Remote Sens. Rev.* **1987**, *2*, 259–387. [[CrossRef](#)]
88. Rees, W.G. *Remote Sensing of Snow and Ice*; CRC Press: Boca Raton, FL, USA, 2005.
89. Rignot, E.; Echelmeyer, K.; Krabill, W. Penetration depth of interferometric synthetic-aperture radar signals in snow and ice. *Geophys. Res. Lett.* **2001**, *28*, 3501–3504. [[CrossRef](#)]
90. Langley, K.; Hamran, S.-E.; Hogda, K.A.; Storvold, R.; Brandt, O.; Hagen, J.O.; Kohler, J. Use of C-Band Ground Penetrating Radar to Determine Backscatter Sources Within Glaciers. *IEEE Trans. Geosci. Remote Sens.* **2007**, *45*, 1236–1246. [[CrossRef](#)]
91. Rott, H.; Mätzler, C. Possibilities and Limits of Synthetic Aperture Radar for Snow and Glacier Surveying. *Ann. Glaciol.* **1987**, *9*, 195–199. [[CrossRef](#)]
92. Shi, J.; Dozier, J. Inferring snow wetness using C-band data from SIR-C's polarimetric synthetic aperture radar. *IEEE Trans. Geosci. Remote Sens.* **1995**, *33*, 905–914.
93. Mätzler, C.; Schanda, E. Snow mapping with active microwave sensors. *Int. J. Remote Sens.* **1984**, *5*, 409–422. [[CrossRef](#)]

94. Ulaby, F.T.; Moore, R.K.; Fung, A.K. *Microwave Remote Sensing: Active and Passive: 3: From Theory to Applications*; Artech House: Norwood, MA, USA, 1986.
95. Ashcraft, I.S.; Long, D.G. Comparison of methods for melt detection over Greenland using active and passive microwave measurements. *Int. J. Remote Sens.* **2006**, *27*, 2469–2488. [[CrossRef](#)]
96. Zhou, C.; Zheng, L. Mapping Radar Glacier Zones and Dry Snow Line in the Antarctic Peninsula Using Sentinel-1 Images. *Remote Sens.* **2017**, *9*, 1171. [[CrossRef](#)]
97. Evans, S. Dielectric Properties of Ice and Snow—A Review. *J. Glaciol.* **1965**, *5*, 773–792. [[CrossRef](#)]
98. Arslan, A.; Wang, H.; Pulliainen, J.; Hallikainen, M. Effective Permittivity of Wet Snow Using Strong Fluctuation Theory—Abstract. *J. Electromagn. Waves Appl.* **2001**, *15*, 53–55. [[CrossRef](#)]
99. Ambach, W.; Denoth, A. *The Dielectric Behaviour of Snow: A Study Versus Liquid Water Content*; NASA: Washington, DC, USA, 1980.
100. Guneriussen, T. Backscattering properties of a wet snow cover derived from DEM corrected ERS-1 SAR data. *Int. J. Remote Sens.* **1997**, *18*, 375–392. [[CrossRef](#)]
101. Strozzi, T.; Matzler, C. Backscattering measurements of alpine snowcovers at 5.3 and 35 GHz. *IEEE Trans. Geosci. Remote Sens.* **1998**, *36*, 838–848. [[CrossRef](#)]
102. Thakur, P.K.; Garg, P.K.; Aggarwal, S.P.; Garg, R.D.; Mani, S. Snow Cover Area Mapping Using Synthetic Aperture Radar in Manali Watershed of Beas River in the Northwest Himalayas. *J. Indian Soc. Remote Sens.* **2013**, *41*, 933–945. [[CrossRef](#)]
103. Guneriussen, T.; Johnsen, H.; Lauknes, I. Snow Cover Mapping Capabilities Using RADARSAT Standard Mode Data. *Can. J. Remote Sens.* **2001**, *27*, 109–117. [[CrossRef](#)]
104. Liu, H.; Wang, L.; Jezek, K. Automated delineation of dry and melt snow zones in Antarctica using active and passive microwave observations from space. *IEEE Trans. Geosci. Remote Sens.* **2006**, *44*, 2152–2163.
105. Chuvieco, E. *Environmental Remote Sensing: Earth Observation from Space*; Ariel: Barcelona, Spain, 2008.
106. Snehmani Singh, M.K.; Gupta, R.D.; Bhardwaj, A.; Joshi, P.K. Remote sensing of mountain snow using active microwave sensors: A review. *Geocarto Int.* **2015**, *30*, 1–27. [[CrossRef](#)]
107. Moghaddam, M.; Saatchi, S. Analysis of scattering mechanisms in SAR imagery over boreal forest: Results from BOREAS. *IEEE Trans. Geosci. Remote Sens.* **1995**, *33*, 1290–1296. [[CrossRef](#)]
108. Eriksson, L.E.; Borenäs, K.; Dierking, W.; Berg, A.; Santoro, M.; Pemberton, P.; Lindh, H.; Karlson, B. Evaluation of new spaceborne SAR sensors for sea-ice monitoring in the Baltic Sea. *Can. J. Remote Sens.* **2010**, *36*, S56–S73. [[CrossRef](#)]
109. Phan, X.-V.; Ferro-Famil, L.; Gay, M.; Durand, Y.; Dumont, M.; Allain, S.; D'Urso, G. Analysis of snowpack properties and structure from TerraSAR-X data, based on multilayer backscattering and snow evolution modeling approaches. *arXiv* **2012**, arXiv:1211.3278.
110. Martini, A.; Ferro-Famil, L.; Pottier, E. Polarimetric study of scattering from dry snow cover in alpine areas. In Proceedings of the 2003 IEEE International Geoscience and Remote Sensing Symposium (IGARSS), Toulouse, France, 21–25 July 2003.
111. Besic, N.; Vasile, G.; Chanussot, J.; Stankovic, S.; Dedieu, J.-P.; d'Urso, G.; Boldo, D.; Ovarlez, J.-P. Dry snow backscattering sensitivity on density change for swe estimation. In Proceedings of the 2012 IEEE International Geoscience and Remote Sensing Symposium (IGARSS), Munich, Germany, 22–27 July 2012.
112. Johansson, A.M.; Brekke, C.; Spreen, G.; King, J.A. X-, C-, and L-band SAR signatures of newly formed sea ice in Arctic leads during winter and spring. *Remote Sens. Environ.* **2018**, *204*, 162–180. [[CrossRef](#)]
113. Schwaizer, G. SAR/Optical Applications to Ice and Snow. In Proceedings of the ESA Training Course on Radar and Optical Remote Sensing, Vilnius, Lithuania, 3–7 July 2017.
114. Shi, J.; Dozier, J. Measurements of snow- and glacier-covered areas with single-polarization SAR. *Ann. Glaciol.* **1993**, *17*, 72–76. [[CrossRef](#)]
115. Bernier, M.; Fortin, J.-P. The potential of times series of C-Band SAR data to monitor dry and shallow snow cover. *IEEE Trans. Geosci. Remote Sens.* **1998**, *36*, 226–243. [[CrossRef](#)]
116. Garrity, C.; Carsey, F.D. Characterization of snow on floating ice and case studies of brightness temperature changes during the onset of melt. *Sea Ice* **1992**, *68*, 313–328.
117. Suzuki, M.; Sasaki, M.; Murata, K.; Fujino, K.; Takeda, K. Evaluation of the data obtained by satellite-borne microwave sensor for snowpack observation. In Proceedings of the International Geoscience and Remote Sensing Symposium, Quantitative Remote Sensing for Science and Applications (IGARSS'95), Firenze, Italy, 10–14 July 1995.

118. Muhuri, A.; Manickam, S.; Bhattacharya, A. Snehmani Snow Cover Mapping Using Polarization Fraction Variation with Temporal RADARSAT-2 C-Band Full-Polarimetric SAR Data Over the Indian Himalayas. *IEEE J. Sel. Top. Appl. Earth Obs. Remote Sens.* **2018**, *11*, 2192–2209. [[CrossRef](#)]
119. Rott, H. The analysis of backscattering properties from SAR data of mountain regions. *IEEE J. Ocean. Eng.* **1984**, *9*, 347–355. [[CrossRef](#)]
120. Rott, H. Synthetic aperture radar capabilities for snow and glacier monitoring. *Adv. Space Res.* **1984**, *4*, 241–246. [[CrossRef](#)]
121. Löw, A.; Ludwig, R.; Mauser, W. Land use dependent snow cover retrieval using multitemporal, multisensoral SAR-images to drive operational flood forecasting models. In Proceedings of the EARSeL-LISSIG-Workshop Observing Our Cryosphere from Space, Bern, Switzerland, 11–13 March 2002.
122. Malenovský, Z.; Rott, H.; Cihlar, J.; Schaepman, M.E.; García-Santos, G.; Fernandes, R.; Berger, M. Sentinels for science: Potential of Sentinel-1, -2, and -3 missions for scientific observations of ocean, cryosphere, and land. *Remote Sens. Environ.* **2012**, *120*, 91–101. [[CrossRef](#)]
123. Attema, E.; Desnos, Y.-L.; Duchossois, G. Synthetic aperture radar in Europe: ERS, Envisat, and beyond. *Johns Hopkins APL Tech. Dig.* **2000**, *21*, 155–161.
124. Strozzi, T. Backscattering Measurements of Snowcovers at 5.3 and 35 ghz; Fakultat der Philosophisch-naturwissenschaftlichen, Universität Bern: Bern, Switzerland, 1996.
125. Venkataraman, G.; Singh, G.; Kumar, V. Snow cover area monitoring using multi-temporal TerraSAR-X data. In Proceedings of the Third TerraSAR-X Science Team Meeting, DLR, Germany, 14–16 February 2008.
126. Nagler, T.; Rott, H. Retrieval of wet snow by means of multitemporal SAR data. *IEEE Trans. Geosci. Remote Sens.* **2000**, *38*, 754–765. [[CrossRef](#)]
127. Rott, H.; Nagler, T. Monitoring temporal dynamics of snowmelt with ERS-1 SAR. In Proceedings of the International Geoscience and Remote Sensing Symposium, Quantitative Remote Sensing for Science and Applications (IGARSS'95), Firenze, Italy, 10–14 July 1995.
128. Notarnicola, C.; Duguay, M.; Moelg, N.; Schellenberger, T.; Tetzlaff, A.; Monsorno, R.; Costa, A.; Steurer, C.; Zebisch, M. Snow Cover Maps from MODIS Images at 250 m Resolution, Part 1: Algorithm Description. *Remote Sens.* **2013**, *5*, 110–126. [[CrossRef](#)]
129. Hall, D.K.; Riggs, G.A. Accuracy assessment of the MODIS snow products. *Hydrol. Process.* **2007**, *21*, 1534–1547. [[CrossRef](#)]
130. Hall, D.K.; Riggs, G.A.; Salomonson, V.V.; Barton, J.; Casey, K.; Chien, J.; DiGirolamo, N.E.; Klein, A.G.; Powell, H.W.; Tait, A.B. Algorithm theoretical basis document (ATBD) for the MODIS snow and sea ice-mapping algorithms. Available online: https://eospso.gsfc.nasa.gov/sites/default/files/atbd/atbd_mod10.pdf (accessed on 17 July 2019).
131. Malnes, E.; Guneriussen, T. Mapping of snow covered area with Radarsat in Norway. In Proceedings of the IEEE International Geoscience and Remote Sensing Symposium (IGARSS'2002), Toronto, ON, Canada, 24–28 June 2002.
132. Longepe, N.; Allain, S.; Ferro-Famil, L.; Pottier, E.; Durand, Y. Snowpack Characterization in Mountainous Regions Using C-Band SAR Data and a Meteorological Model. *IEEE Trans. Geosci. Remote Sens.* **2009**, *47*, 406–418. [[CrossRef](#)]
133. Pettinato, S.; Malnes, E.; Haarpaintner, J. Snow cover maps with satellite borne SAR: A new approach in harmony with fractional optical SCA retrieval algorithms. In Proceedings of the IEEE International Geoscience and Remote Sensing Symposium (IGARSS), Denver, CO, USA, 31 July–4 August 2006.
134. Schellenberger, T.; Ventura, B.; Zebisch, M.; Notarnicola, C. Wet Snow Cover Mapping Algorithm Based on Multitemporal COSMO-SkyMed X-Band SAR Images. *IEEE J. Sel. Top. Appl. Earth Obs. Remote Sens.* **2012**, *5*, 1045–1053. [[CrossRef](#)]
135. Baghdadi, N. Capability of Multitemporal ERS-1 SAR Data for Wet-Snow Mapping. *Remote Sens. Environ.* **1997**, *60*, 174–186. [[CrossRef](#)]
136. Pettinato, S.; Santi, E.; Paloscia, S.; Aiazzi, B.; Baronti, S.; Garzelli, A. Snow cover area identification by using a change detection method applied to COSMO-SkyMed images. *J. Appl. Remote Sens.* **2014**, *8*, 84684. [[CrossRef](#)]

137. Ventura, B.; Schellenberger, T.; Notarnicola, C.; Zebisch, M.; Nagler, T.; Rott, H.; Maddalena, V.; Ratti, R.; Tampellini, L. Snow cover monitoring in alpine regions with cosmo-skymed images by using a multitemporal approach and depolarization ratio. In Proceedings of the 2011 6th International Workshop on the Analysis of Multi-Temporal Remote Sensing Images (Multi-Temp), Trento, Italy, 12–14 July 2011.
138. Koskinen, J.; Pulliainen, J.; Hallikainen, M. The use of ERS-1 SAR data in snow melt monitoring. *IEEE Trans. Geosci. Remote Sens.* **1997**, *35*, 601–610. [[CrossRef](#)]
139. Luojus, K.; Pulliainen, J.; Metsamaki, S.; Hallikainen, M. Accuracy assessment of SAR data-based snow-covered area estimation method. *IEEE Trans. Geosci. Remote Sens.* **2006**, *44*, 277–287. [[CrossRef](#)]
140. Nagler, T.; Rott, H.; Ripper, E.; Bippus, G.; Hetzenegger, M. Advancements for Snowmelt Monitoring by Means of Sentinel-1 SAR. *Remote Sens.* **2016**, *8*, 348. [[CrossRef](#)]
141. Magagi, R.; Bernier, M. Optimal conditions for wet snow detection using RADARSAT SAR data. *Remote Sens. Environ.* **2003**, *84*, 221–233. [[CrossRef](#)]
142. Rao, Y.; Venkataraman, G.; Singh, G. ENVISAT-ASAR data analysis for snow cover mapping over Gangotri region. In Proceedings of the Microwave Remote Sensing of the Atmosphere and Environment V, Goa, India, 13–17 November 2006.
143. Tsai YL, S.; Dietz, A.; Oppelt, N.; Kuenzer, C. Wet and Dry Snow Detection Using Sentinel-1 SAR Data for Mountainous Areas with a Machine Learning Technique. *Remote Sens.* **2019**, *11*, 895. [[CrossRef](#)]
144. Wang, Y.; Wang, L.; Li, H.; Yang, Y.; Yang, T. Assessment of Snow Status Changes Using L-HH Temporal-Coherence Components at Mt. Dagu, China. *Remote Sens.* **2015**, *7*, 11602–11620. [[CrossRef](#)]
145. Singh, G.; Venkataraman, G.; Rao, Y.S.; Kumar, V. InSAR coherence measurement techniques for snow cover mapping in Himalayan region. In Proceedings of the IEEE International Geoscience and Remote Sensing Symposium (IGARSS), Boston, MA, USA, 8–11 July 2008.
146. Shi, J.; Hensley, S.; Dozier, J. Mapping snow cover with repeat pass synthetic aperture radar. In Proceedings of the 1997 IEEE International Geoscience and Remote Sensing Symposium Proceedings. Remote Sensing—A Scientific Vision for Sustainable Development, Singapore, 3–8 August 1997.
147. Strozzi, T.; Wegmüller, U.; Mätzler, C. Mapping wet snowcovers with SAR interferometry. *Int. J. Remote Sens.* **1999**, *20*, 2395–2403. [[CrossRef](#)]
148. Guo, C.; Tong, L.; Chen, Y.; Yang, X. Snow extraction using X-band multi-temporal coherence based on insar technology. In Proceedings of the 2017 IEEE International Geoscience and Remote Sensing Symposium (IGARSS), Fort Worth, TX, USA, 23–28 July 2017.
149. Guangjun, H.; Pengfeng, X.; Xuezhi, F.; Xueliang, Z.; Zuo, W.; Ni, C. Extracting Snow Cover in Mountain Areas Based on SAR and Optical Data. *IEEE Geosci. Remote Sens. Lett.* **2015**, *12*, 1136–1140. [[CrossRef](#)]
150. Zebker, H.; Villasenor, J. Decorrelation in interferometric radar echoes. *IEEE Trans. Geosci. Remote Sens.* **1992**, *30*, 950–959. [[CrossRef](#)]
151. Malnes, E.; Storvold, R.; Lauknes, I. Near real time snow covered area mapping with Envisat ASAR wideswath in Norwegian mountainous areas. In Proceedings of the ESA ENVISAT & ERS Symposium, Salzburg, Austria, 6–10 September 2004.
152. Thakur, P.K.; Aggarwal, S.P.; Arun, G.; Sood, S.; Kumar, A.S.; Mani, S.; Dobhal, D.P. Estimation of Snow Cover Area, Snow Physical Properties and Glacier Classification in Parts of Western Himalayas Using C-Band SAR Data. *J. Indian Soc. Remote Sens.* **2016**, *45*, 525–539. [[CrossRef](#)]
153. Ji, X.; Chen, Y.; Tong, L.; Jia, M.; Tan, L.; Fan, S. Area retrieval of melting snow in alpine areas. In Proceedings of the 2014 IEEE International Geoscience and Remote Sensing Symposium (IGARSS), Quebec City, QC, Canada, 13–18 July 2014.
154. Storvold, R.; Malnes, E. Snow covered area retrieval using ENVISAT ASAR wideswath in mountainous areas. In Proceedings of the 2004 IEEE International Geoscience and Remote Sensing Symposium (IGARSS), Anchorage, AK, USA, 20–24 September 2004.
155. Pettinato, S.; Poggi, P.; Macelloni, G.; Paloscia, S.; Pampaloni, P.; Crepaz, A. Mapping snow cover in alpine areas with ENVISAT/SAR images. In Proceedings of the ESA ENVISAT & ERS Symposium, Salzburg, Austria, 6–10 September 2004.
156. Brogioni, M.; Macelloni, G.; Paloscia, S.; Pampaloni, P.; Pettinato, S.; Santi, E. Monitoring snow cover characteristics with multifrequency active and passive microwave sensors. In Proceedings of the IEEE International Geoscience and Remote Sensing Symposium (IGARSS), Beijing, China, 10–15 July 2016.

157. Rott, H. Thematic studies in alpine areas by means of polarimetric SAR and optical imagery. *Adv. Space Res.* **1994**, *14*, 217–226. [[CrossRef](#)]
158. Shi, J.; Dozier, J. Mapping seasonal snow with SIR-C/X-SAR in mountainous areas. *Remote Sens. Environ.* **1997**, *59*, 294–307. [[CrossRef](#)]
159. Muhuri, A.; Ratha, D.; Bhattacharya, A. Seasonal Snow Cover Change Detection Over the Indian Himalayas Using Polarimetric SAR Images. *IEEE Geosci. Remote Sens. Lett.* **2017**, *14*, 2340–2344. [[CrossRef](#)]
160. Cloude, S.; Pottier, E. A review of target decomposition theorems in radar polarimetry. *IEEE Trans. Geosci. Remote Sens.* **1996**, *34*, 498–518. [[CrossRef](#)]
161. Touzi, R.; Boerner, W.M.; Lee, J.S.; Lueneburg, E. A review of polarimetry in the context of synthetic aperture radar: Concepts and information extraction. *Can. J. Remote Sens.* **2004**, *30*, 380–407. [[CrossRef](#)]
162. Zhang, L.; Zou, B.; Cai, H.; Zhang, Y. Multiple-Component Scattering Model for Polarimetric SAR Image Decomposition. *IEEE Geosci. Remote Sens. Lett.* **2008**, *5*, 603–607. [[CrossRef](#)]
163. He, G.; Feng, X.; Xia, Z.; Guo, J.; Xiao, P.; Wang, Z.; Chen, H.; Li, H. Dry and Wet Snow Cover Mapping in Mountain Areas Using SAR and Optical Remote Sensing Data. *IEEE J. Sel. Top. Appl. Earth Obs. Remote Sens.* **2017**, *10*, 2575–2588. [[CrossRef](#)]
164. Bruzzone, L.; Roli, F.; Serpico, S. An extension of the Jeffreys-Matusita distance to multiclass cases for feature selection. *IEEE Trans. Geosci. Remote Sens.* **1995**, *33*, 1318–1321. [[CrossRef](#)]
165. Huang, L.; Li, Z.; Tian, B.-S.; Chen, Q.; Liu, J.-L.; Zhang, R. Classification and snow line detection for glacial areas using the polarimetric SAR image. *Remote Sens. Environ.* **2011**, *115*, 1721–1732. [[CrossRef](#)]
166. Baghdadi, N.; Livingstone, C.; Bernier, M. Airborne C-band SAR measurements of wet snow-covered areas. *IEEE Trans. Geosci. Remote Sens.* **1998**, *36*, 1977–1981. [[CrossRef](#)]
167. Reppucci, A.; Banque, X.; Zhan, Y.; Alonso, A.; Lopez-Martinez, C. Estimation of snow pack characteristics by means of polarimetric SAR data. *SPIE Remote Sens.* **2012**, *8531*, 85310.
168. Muhuri, A.; Manickam, S.; Bhattacharya, A. Scattering Mechanism Based Snow Cover Mapping Using RADARSAT-2 C-Band Polarimetric SAR Data. *IEEE J. Sel. Top. Appl. Earth Obs. Remote Sens.* **2017**, *10*, 3213–3224. [[CrossRef](#)]
169. Park, S.-E.; Yamaguchi, Y.; Singh, G.; Yamaguchi, S.; Whitaker, A.C. Polarimetric SAR Response of Snow-Covered Area Observed by Multi-Temporal ALOS PALSAR Fully Polarimetric Mode. *IEEE Trans. Geosci. Remote Sens.* **2014**, *52*, 329–340. [[CrossRef](#)]
170. Venkataraman, G.; Singh, G.; Yamaguchi, Y. Fully polarimetric ALOS PALSAR data applications for snow and ice studies. In Proceedings of the IGARSS 2010—2010 IEEE International Geoscience and Remote Sensing Symposium, Honolulu, HI, USA, 25–30 July 2010; pp. 1776–1779.
171. Venkataraman, G.; Singh, G.; Yamaguchi, Y.; Park, S.-E. Methodology development for snow discrimination using SAR polarimetry techniques. In Proceedings of the 2011 3rd International Asia-Pacific Conference on Synthetic Aperture Radar (APSAR), Seoul, Korea, 26–30 September 2011.
172. Martini, A.; Ferro-Famil, L.; Pottier, E.; Dedieu, J.-P. Dry snow discrimination in alpine areas from multi-frequency and multi-temporal SAR data. *IEE Proc. Radar Sonar Navig.* **2006**, *153*, 271–278. [[CrossRef](#)]
173. Camps-Valls, G.; Bruzzone, L. Kernel-based methods for hyperspectral image classification. *IEEE Trans. Geosci. Remote Sens.* **2005**, *43*, 1351–1362. [[CrossRef](#)]
174. Longepe, N.; Shimada, M.; Allain, S.; Pottier, E. Capabilities of full-polarimetric PALSAR/ALOS for snow extent mapping. In Proceedings of the IEEE International Geoscience and Remote Sensing Symposium (IGARSS), Boston, MA, USA, 8–11 July 2008.
175. Luoju, K.P.; Pulliainen, J.T.; Metsamaki, S.J.; Hallikainen, M.T. Snow-Covered Area Estimation Using Satellite Radar Wide-Swath Images. *IEEE Trans. Geosci. Remote Sens.* **2007**, *45*, 978–989. [[CrossRef](#)]
176. Haefner, H. Small-Scale Monitoring of Wet Snowcover with Radarsat-ScanSAR Data. *EARSeL eProceedings* **2001**, *1*, 339–346.
177. Li, Z.; Huang, L.; Chen, Q.; Tian, B.S. Glacier Snow Line Detection on a Polarimetric SAR Image. *IEEE Geosci. Remote Sens. Lett.* **2012**, *9*, 584–588.
178. Small, D. Flattening Gamma: Radiometric Terrain Correction for SAR Imagery. *IEEE Trans. Geosci. Remote Sens.* **2011**, *49*, 3081–3093. [[CrossRef](#)]
179. Baghdadi, N.; Gauthier, Y.; Bernier, M.; Fortin, J.-P. Potential and limitations of RADARSAT SAR data for wet snow monitoring. *IEEE Trans. Geosci. Remote Sens.* **2000**, *38*, 316–320. [[CrossRef](#)]

180. Usami, N.; Muhuri, A.; Bhattacharya, A.; Hirose, A. PolSAR Wet Snow Mapping with Incidence Angle Information. *IEEE Geosci. Remote Sens. Lett.* **2016**, *13*, 2029–2033. [[CrossRef](#)]
181. Holah, N.; Baghdadi, N.; Zribi, M.; Bruand, A.; King, C. Potential of ASAR/ENVISAT for the characterization of soil surface parameters over bare agricultural fields. *Remote Sens. Environ.* **2005**, *96*, 78–86. [[CrossRef](#)]
182. Karam, M.A.; Amar, F.; Fung, A.K.; Mougin, E.; Lopès, A.; Le Vine, D.M.; Beaudoin, A. A microwave polarimetric scattering model for forest canopies based on vector radiative transfer theory. *Remote Sens. Environ.* **1995**, *53*, 16–30. [[CrossRef](#)]
183. Pulliainen, J.T. Investigation on the Backscattering Properties of Finnish Boreal Forests at C-and X-Band: A Semi-Empirical Modeling Approach. Ph.D. Thesis, Laboratory of Space Technology, Helsinki University of Technology, Espoo, Finland, 1994.
184. Duguay, Y.; Bernier, M. The use of RADARSAT-2 and TerraSAR-X data for the evaluation of snow characteristics in subarctic regions. In Proceedings of the 2012 IEEE International Geoscience and Remote Sensing Symposium (IGARSS), Munich, Germany, 22–27 July 2012.
185. Kumar, V.; Venkataraman, G. SAR interferometric coherence analysis for snow cover mapping in the western Himalayan region. *Int. J. Digit. Earth* **2011**, *4*, 78–90. [[CrossRef](#)]
186. Notarnicola, C.; Ratti, R.; Maddalena, V.; Schellenberger, T.; Ventura, B.; Zebisch, M. Seasonal Snow Cover Mapping in Alpine Areas Through Time Series of COSMO-SkyMed Images. *IEEE Geosci. Remote Sens. Lett.* **2013**, *10*, 716–720. [[CrossRef](#)]
187. Notarnicola, C.; Schellenberger, T.; Ventura, B.; Zebisch, M.; Maddalena, V.; Ratti, R.; Tampellini, L. Time series analysis of dual-pol COSMO-SkyMed images for monitoring snow cover in alpine areas. In Proceedings of the 2012 IEEE International Geoscience and Remote Sensing Symposium (IGARSS), Munich, Germany, 22–27 July 2012.
188. Paloscia, S.; Pettinato, S.; Santi, E.; Valt, M. COSMO-SkyMed Image Investigation of Snow Features in Alpine Environment. *Sensors* **2017**, *17*, 84. [[CrossRef](#)] [[PubMed](#)]
189. Luojus, K.; Pulliainen, J.; Metsamaki, S.; Hallikainen, M. Enhanced SAR-Based Snow-Covered Area Estimation Method for Boreal Forest Zone. *IEEE Trans. Geosci. Remote Sens.* **2009**, *47*, 922–935. [[CrossRef](#)]
190. Rott, H.; Cline, D.; Nagler, T.; Pulliainen, J.; Rebhan, H.; Yueh, S. CoReH2O-A dual frequency SAR mission for hydrology and climate research. In Proceedings of the IEEE International Geoscience and Remote Sensing Symposium (IGARSS), Barcelona, Spain, 23–28 July 2007.
191. Callegari, M.; Carturan, L.; Marin, C.; Notarnicola, C.; Rastner, P.; Seppi, R.; Zucca, F. A Pol-SAR Analysis for Alpine Glacier Classification and Snowline Altitude Retrieval. *IEEE J. Sel. Top. Appl. Earth Obs. Remote Sens.* **2016**, *9*, 3106–3121. [[CrossRef](#)]
192. Rott, H.; Davis, R.E. Multi-parameter airborne SAR experiments at an alpine test site. In Proceedings of the International Geoscience and Remote Sensing Symposium Remote Sensing: Global Monitoring for Earth Management, Espoo, Finland, 3–6 June 1991.
193. Martone, M.; Bräutigam, B.; Krieger, G. Decorrelation effects in bistatic TanDEM-X data. In Proceedings of the 2012 IEEE International Geoscience and Remote Sensing Symposium (IGARSS), Munich, Germany, 22–27 July 2012.
194. Rizzoli, P.; Martone, M.; Rott, H.; Moreira, A. Characterization of Snow Facies on the Greenland Ice Sheet Observed by TanDEM-X Interferometric SAR Data. *Remote Sens.* **2017**, *9*, 315. [[CrossRef](#)]
195. Nagler, T.; Rott, H. Snow classification algorithm for Envisat ASAR. In Proceedings of the ESA ENVISAT & ERS Symposium, Salzburg, Austria, 6–10 September 2004.
196. Dedieu, J.-P.; Besic, N.; Vasile, G.; Mathieu, J.; Durand, Y.; Gottardi, F. Dry snow analysis in alpine regions using RADARSAT-2 full polarimetry data. Comparison with in situ measurements. In Proceedings of the 2014 IEEE International Geoscience and Remote Sensing Symposium (IGARSS), Quebec City, QC, Canada, 13–18 July 2014.
197. Baghdadi, N.; Fortin, J.-P.; Bernier, M. Accuracy of wet snow mapping using simulated Radarsat backscattering coefficients from observed snow cover characteristics. *Int. J. Remote Sens.* **1999**, *20*, 2049–2068. [[CrossRef](#)]
198. Nijhawan, R.; Das, J.; Raman, B. A hybrid of deep learning and hand-crafted features based approach for snow cover mapping. *Int. J. Remote Sens.* **2018**, *40*, 759–773. [[CrossRef](#)]
199. Luojus, K.; Pulliainen, J.; Cutrona, A.B.; Metsamaki, S.; Hallikainen, M. Comparison of SAR-Based Snow-Covered Area Estimation Methods for the Boreal Forest Zone. *IEEE Geosci. Remote Sens. Lett.* **2009**, *6*, 403–407. [[CrossRef](#)]

200. Luojus, K.; Kärnä, J.-P.; Hallikainen, M.; Pulliainen, J. Development of techniques to retrieve Snow Covered Area (SCA) in boreal forests from space-borne microwave observations. In Proceedings of the IGARSS IEEE International Conference on the Geoscience and Remote Sensing Symposium, Denver, CO, USA, 31 July–4 August 2006.
201. Kaasalainen, S.; Holopainen, M.; Karjalainen, M.; Vastaranta, M.; Kankare, V.; Karila, K.; Osmanoğlu, B. Combining Lidar and Synthetic Aperture Radar Data to Estimate Forest Biomass: Status and Prospects. *Forests* **2015**, *6*, 252–270. [[CrossRef](#)]
202. Sinha, S.; Jeganathan, C.; Sharma, L.K.; Nathawat, M.S. A review of radar remote sensing for biomass estimation. *Int. J. Environ. Sci. Technol.* **2015**, *12*, 1779–1792. [[CrossRef](#)]
203. Minh, D.H.T.; Le Toan, T.; Rocca, F.; Tebaldini, S.; D’Alessandro, M.M.; Villard, L. Relating P-Band Synthetic Aperture Radar Tomography to Tropical Forest Biomass. *IEEE Trans. Geosci. Remote Sens.* **2014**, *52*, 967–979. [[CrossRef](#)]
204. Heliere, F.; Fois, F.; Arcioni, M.; Bensi, P.; Fehringer, M.; Scipal, K. Biomass P-band SAR interferometric mission selected as 7th Earth Explorer Mission. In Proceedings of the 10th European Conference on Synthetic Aperture Radar (EUSAR 2014), Berlin, Germany, 3–5 June 2014.
205. Lessard-Fontaine, A.; Allain, S.; Dedieu, J.-P.; Durand, Y. Multi-temporal wet snow mapping in alpine context using polarimetric Radarsat-2 time-series. In Proceedings of the 2012 IEEE International Geoscience and Remote Sensing Symposium (IGARSS), Munich, Germany, 22–27 July 2012.
206. Huang, L.; Li, Z.; Tian, B.-S.; Chen, Q.; Zhou, J.-M. Monitoring glacier zones and snow/firn line changes in the Qinghai–Tibetan Plateau using C-band SAR imagery. *Remote Sens. Environ.* **2013**, *137*, 17–30. [[CrossRef](#)]
207. Nagler, T. *Methods and Analysis of Synthetic Aperture Radar Data from ERS-1 and X-SAR for Snow and Glacier Applications*; Leopold-Franzens-Universität Innsbruck: Innsbruck, Austria, 1996.
208. He, G.; Jiang, J.; Xia, Z.; Hao, Y.; Xiao, P.; Feng, X.; Wang, Z. Snow cover extraction in mountain areas using RadarSat-2 polarimetric SAR data. In Proceedings of the 2016 16th International Conference on Ground Penetrating Radar (GPR), Hong Kong, China, 13–16 June 2016.
209. Wendleder, A.; Heilig, A.; Schmitt, A.; Mayer, C. Monitoring of Wet Snow and Accumulations at High Alpine Glaciers Using Radar Technologies. *Int. Arch. Photogramm. Remote Sens. Spat. Inf. Sci.* **2015**, *40*, 1063. [[CrossRef](#)]
210. Tso, B.; Mather, P.M. Crop discrimination using multi-temporal SAR imagery. *Int. J. Remote Sens.* **1999**, *20*, 2443–2460. [[CrossRef](#)]
211. Singh, G.; Venkataraman, G. Application of incoherent target decomposition theorems to classify snow cover over the Himalayan region. *Int. J. Remote Sens.* **2012**, *33*, 4161–4177. [[CrossRef](#)]
212. Crawford, C.J.; Manson, S.M.; Bauer, M.E.; Hall, D.K. Multitemporal snow cover mapping in mountainous terrain for Landsat climate data record development. *Remote Sens. Environ.* **2013**, *135*, 224–233. [[CrossRef](#)]
213. Crawford, C.J. MODIS Terra Collection 6 fractional snow cover validation in mountainous terrain during spring snowmelt using Landsat TM and ETM+. *Hydrol. Process.* **2015**, *29*, 128–138. [[CrossRef](#)]
214. Winther, J.-G.; Hall, D.K. Satellite-derived snow coverage related to hydropower production in Norway: Present and future. *Int. J. Remote Sens.* **1999**, *20*, 2991–3008. [[CrossRef](#)]
215. Xiao, X.; Zhang, Q.; Boles, S.; Rawlins, M.; Moore, B. Mapping snow cover in the pan-Arctic zone, using multi-year (1998–2001) images from optical VEGETATION sensor. *Int. J. Remote Sens.* **2004**, *25*, 5731–5744. [[CrossRef](#)]
216. Klein, A.G.; Hall, D.K.; Riggs, G.A. Improving snow cover mapping in forests through the use of a canopy reflectance model. *Hydrol. Process.* **1998**, *12*, 1723–1744. [[CrossRef](#)]
217. Lehning, M.; Bartelt, P.; Brown, B.; Fierz, C.; Satyawali, P. A physical SNOWPACK model for the Swiss avalanche warning: Part II. Snow microstructure. *Cold Reg. Sci. Tech.* **2002**, *35*, 147–167. [[CrossRef](#)]
218. Krol, Q.; Löwe, H. Analysis of local ice crystal growth in snow. *J. Glaciol.* **2016**, *62*, 378–390. [[CrossRef](#)]
219. Mätzler, C.; Strozzi, T.; Wiesmann, A. Active microwave signatures of snow covers at 5.3 and 35 GHz. *Radio Sci.* **1997**, *32*, 479–495.
220. Pettinato, S.; Santi, E.; Paloscia, S. Investigation of alpine snow features using cosmo-skymed images. In Proceedings of the 2017 IEEE International Geoscience and Remote Sensing Symposium (IGARSS), Fort Worth, TX, USA, 23–28 July 2017.

221. Nagler, T.; Rott, H.; Ossowska, J.; Schwaizer, G.; Small, D.; Malnes, E.; Luojus, K.; Metsämäki, S.; Pinnock, S. Snow Cover Monitoring by Synergistic Use of Sentinel-3 Slstr and Sentinel-L Sar Data. In Proceedings of the 2018 IEEE International Geoscience and Remote Sensing Symposium (IGARSS 2018), Valencia, Spain, 22–27 July 2018.
222. Snipir, B.; Momblanch, A.; Jain, S.; Waine, T.; Holman, I. A method for monthly mapping of wet and dry snow using Sentinel-1 and MODIS: Application to a Himalayan river basin. *Int. J. Appl. Earth Obs. Geoinf.* **2019**, *74*, 222–230. [[CrossRef](#)]
223. Dozier, J.; Shi, J. Estimation of snow water equivalence using SIR-C/X-SAR. II. Inferring snow depth and particle size. *IEEE Trans. Geosci. Remote Sens.* **2000**, *38*, 2475–2488. [[CrossRef](#)]
224. Singh, G.; Kumar, V.; Mohite, K.; Venkatraman, G.; Rao, Y. Snow wetness estimation in Himalayan snow covered regions using ENVISAT-ASAR data. In Proceedings of the Microwave Remote Sensing of the Atmosphere and Environment V, Goa, India, 13–17 November 2006.
225. Niang, M.; Dedieu, J.-P.; Durand, Y.; Mérindol, L.; Bernier, M.; Dumont, M. New inversion method for snow density and snow liquid water content retrieval using C-band data from ENVISAT/ASAR alternating polarization in alpine environment. In Proceedings of the Envisat Symposium, Montreux, Switzerland, 23–27 April 2007.
226. Ventura, B.; Schellenberger, T.; Notarnicola, C.; Zebisch, M.; Maddalena, V.; Ratti, R.; Tampellini, L.; Du, J. Analysis of snow changes in alpine regions with X-band data: Electromagnetic analysis and snow cover mapping. *SPIE Remote Sens.* **2011**, *8179*, 817908.
227. Besic, N.; Vasile, G.; Chanussot, J.; Stankovic, S.; Ovarlez, J.-P.; d’Urso, G.; Boldo, D.; Dedieu, J.-P. Stochastically based wet snow mapping with SAR data. In Proceedings of the 2012 IEEE International Geoscience and Remote Sensing Symposium (IGARSS), Munich, Germany, 22–27 July 2012.
228. Rizzoli, P.; Martone, M.; Brautigam, B. Greenland ice sheet snow facies identification approach using TanDEM-X interferometric data. In Proceedings of the 2015 IEEE International Geoscience and Remote Sensing Symposium (IGARSS), Milan, Italy, 26–31 July 2015.
229. Rizzoli, P.; Martone, M.; Brautigam, B.; Rott, H.; Moreira, A. Multi-Temporal Investigation of Greenland Ice Sheet Snow Facies using TanDEM-X Mission Data. In Proceedings of the Living Planet Symposium, Prague, Czech Republic, 9–13 May 2016.
230. Koskinen, J.; Pulliainen, J.; Luojus, K.; Takala, M. Monitoring of Snow-Cover Properties During the Spring Melting Period in Forested Areas. *IEEE Trans. Geosci. Remote Sens.* **2010**, *48*, 50–58. [[CrossRef](#)]
231. Tampellini, M.L. Monitoring of Glacier and Snow Cover Changes in Alpine Region using Remote Sensing Data. In Proceedings of the 54th International Astronautical Congress of the International Astronautical Federation, Bremen, Germany, 29 September–3 October 2003.
232. Li, Z.; Guo, H.; Li, X.; Wang, C. SAR Interferometry coherence analysis for snow mapping. In Proceedings of the IEEE 2001 International Geoscience and Remote Sensing Symposium (IGARSS), Sydney, Australia, 9–13 July 2001.
233. Haefner, H.; Small, D.; Biegger, S.; Hoffmann, H.; Nuesch, D. Estimation of snow cover over large mountainous areas using Radarsat ScanSAR. In Proceedings of the Remote Sensing and Hydrology, Santa Fe, NM, USA, April 2000.
234. Anttila, S.; Metsämäki, S.; Pulliainen, J.; Luojus, K. From EO data to snow covered area (SCA) end products using automated processing system. In Proceedings of the 2005 IEEE International Geoscience and Remote Sensing Symposium (IGARSS), Seoul, Korea, 25–29 July 2005.
235. Luojus, K.; Pulliainen, J.; Metsämäki, S. Evaluation of the single reference image snow-covered area estimation method for the boreal forest zone. In Proceedings of the 2009 IEEE International Geoscience and Remote Sensing Symposium (IGARSS 2009), Cape Town, South Africa, 12–17 July 2009.
236. Luojus, K.; Pulliainen, J.; Metsämäki, S.; Molera, G.; Nakari, R.; Kärnä, J.-P.; Hallikainen, M. Development of sar-based snow-covered area estimation method for borel forest zone. In Proceedings of the IEEE International Geoscience and Remote Sensing Symposium (IGARSS), Boston, MA, USA, 7–11 July 2008.
237. Storvold, R.; Malnes, E.; Lauknes, I. Using ENVISAT ASAR wideswath data to retrieve snow covered area in mountainous regions. *EARSeL eProceedings* **2006**, *4*, 150–156.
238. Pettianato, S.; Santi, E.; Brogioni, M.; Macelloni, G.; Paloscia, S.; Pampaloni, P. An operational algorithm for snow cover mapping by using optical and SAR data. In Proceedings of the ESA Living Planet Symposium, Bergen, Norway, 28 June–2 July 2010.

239. Longépé, N.; Allain, S.; Pottier, E. Toward an Operational Method for Refined Snow Characterization Using Dual-Polarization C-Band SAR Data. In Proceedings of the IEEE International Geoscience and Remote Sensing Symposium (IGARSS), Boston, MA, USA, 7–11 July 2008.
240. Solberg, R.; Koren, H.; Malnes, E.; Haarpaintner, J.; Lauknes, I. An approach for multisensor harmonization in snow cover area mapping. In Proceedings of the IGARSS IEEE International Conference on Geoscience and Remote Sensing Symposium, Denver, CO, USA, 31 July–4 August 2006.
241. Pettinato, S.; Santi, E.; Brogioni, M.; Paloscia, S.; Pampaloni, P. An operational algorithm for snow cover mapping in hydrological applications. In Proceedings of the 2009 IEEE International Geoscience and Remote Sensing Symposium (IGARSS 2009), Cape Town, South Africa, 12–17 July 2009.
242. Valenti, L.; Small, D.; Meier, E. Snow cover monitoring using multi-temporal Envisat/ASAR data. In Proceedings of the 5th EARSeL LISSIG (Land, Ice, Snow) Workshop, Bern, Switzerland, 11–13 February 2008.
243. Solberg, R.; Huseby, R.B.; Koren, H.; Malnes, E. Time-series fusion of optical and SAR data for snow cover area mapping. In Proceedings of the 5th EARSeL LIS-SIG Workshop: Remote Sensing of Land Ice and Snow, Bern, Switzerland, 11–13 February 2008.
244. Pettinato, S.; Santi, E.; Brogioni, M.; Macelloni, G.; Paloscia, S.; Pampaloni, P. Snow cover mapping by using optical and SAR data. In Proceedings of the Image and Signal Processing for Remote Sensing XV, Berlin, Germany, 31 August–2 September 2009.
245. Solberg, R.; Amlien, J.; Koren, H.; Eikvil, L.; Malnes, E.; Storvold, R. Multi-sensor and time-series approaches for monitoring of snow parameters. In Proceedings of the 2004 IEEE International Geoscience and Remote Sensing Symposium (IGARSS), Anchorage, AK, USA, 20–24 September 2004.
246. He, G.; Hao, Y.; Xiao, P.; Feng, X.; Li, H.; Wang, Z. Snow recognition in mountain areas based on SAR and optical remote sensing data. In Proceedings of the 2016 IEEE International Geoscience and Remote Sensing Symposium (IGARSS), Beijing, China, 10–15 July 2016.
247. Pratola, C.; Navarro-Sánchez, V.D. Snow Cover Monitoring in Hardangervidda and Sierra Nevada Protected Areas by using Sentinel-L Time Series. In Proceedings of the 2018 IEEE International Geoscience and Remote Sensing Symposium (IGARSS 2018), Valencia, Spain, 22–27 July 2018.
248. Wendleder, A.; Dietz, A.J.; Schork, K. Mapping Snow Cover Extent Using Optical and SAR Data. In Proceedings of the 2018 IEEE International Geoscience and Remote Sensing Symposium (IGARSS 2018), Valencia, Spain, 22–27 July 2018.
249. Thakur, P.; Garg, V.; Nikam, B.; Singh, S.; Chouksey, A.; Dhote, P.; Aggarwal, S.; Chauhan, P.; Kumar, A. Snow cover and glacier dynamics study using c-and l-band SAR datasets in parts of North West Himalaya. In Proceedings of the International Archives of the Photogrammetry, Remote Sensing & Spatial Information Sciences, Dehradun, India, 20–23 November 2018.
250. Wang, S.; Yang, B.; Zhou, Y.; Wang, F.; Zhang, R.; Zhao, Q. Snow Cover Mapping and Ice Avalanche Monitoring from the Satellite Data of the Sentinels. *ISPRS Int. Arch. Photogramm. Remote Sens. Spat. Inf. Sci.* **2018**, *42*, 1765–1772. [[CrossRef](#)]
251. Singh, G.; Yamaguchi, Y.; Venktaraman, G.; Park, S.-E. Potential assessment of SAR in compact and full polarimetry mode for snow detection. In Proceedings of the 2011 IEEE International Geoscience and Remote Sensing Symposium (IGARSS), Vancouver, BC, Canada, 24–29 July 2011.
252. Singh, G.; Venkataraman, G.; Rao, Y. The H/A/Alpha polarimetric decomposition theorem and complex wishart distribution for snow cover monitoring. In Proceedings of the IEEE International Geoscience and Remote Sensing Symposium (IGARSS), Boston, MA, USA, 8–11 July 2008.
253. Freeman, A.; Durden, S. A three-component scattering model for polarimetric SAR data. *IEEE Trans. Geosci. Remote Sens.* **1998**, *36*, 963–973. [[CrossRef](#)]
254. Yamaguchi, Y.; Yajima, Y.; Yamada, H. A Four-Component Decomposition of POLSAR Images Based on the Coherency Matrix. *IEEE Geosci. Remote Sens. Lett.* **2006**, *3*, 292–296. [[CrossRef](#)]
255. Touzi, R. Target Scattering Decomposition in Terms of Roll-Invariant Target Parameters. *IEEE Trans. Geosci. Remote Sens.* **2007**, *45*, 73–84. [[CrossRef](#)]
256. Antropov, O.; Rauste, Y.; Hame, T. Volume Scattering Modeling in PolSAR Decompositions: Study of ALOS PALSAR Data Over Boreal Forest. *IEEE Trans. Geosci. Remote Sens.* **2011**, *49*, 3838–3848. [[CrossRef](#)]

257. Schmitt, A.; Wendleder, A.; Hinz, S. The Kennaugh element framework for multi-scale, multi-polarized, multi-temporal and multi-frequency SAR image preparation. *ISPRS J. Photogramm. Remote Sens.* **2015**, *102*, 122–139. [[CrossRef](#)]
258. Van Zyl, J.J.; Zebker, H.A.; Elachi, C. Imaging radar polarization signatures: Theory and observation. *Radio Sci.* **1987**, *22*, 529–543. [[CrossRef](#)]
259. Ainsworth, T.; Cloude, S.; Lee, J. Eigenvector analysis of polarimetric SAR data. In Proceedings of the 2002 IEEE International Geoscience and Remote Sensing Symposium (IGARSS), Toronto, ON, Canada, 24–28 June 2002.
260. Lüneburg, E. *Foundations of the Mathematical Theory of Polarimetry*; Final Report Phase; EML Consultants: Sri Jayawardenepura Kotte, Sri Lanka, July 2001.
261. Allain, S.; Ferro-Famil, L.; Pottier, E. A polarimetric classification from PolSAR data using SERD/DERD parameters. In Proceedings of the 6th European Conference on Synthetic Aperture Radar (EUSAR 2006), Dresden, Germany, 16–18 May 2006.
262. Lee, J.; Pottier, E. *Polarimetric Radar Imaging: From Basics to Applications*; CRC Press: Boca Raton, FL, USA, 2009.



© 2019 by the authors. Licensee MDPI, Basel, Switzerland. This article is an open access article distributed under the terms and conditions of the Creative Commons Attribution (CC BY) license (<http://creativecommons.org/licenses/by/4.0/>).